How does the Rotational Velocity of the Milky Way Galaxy at Different Radii Correlate to its Expected Mass Distribution?

– Extended Project

Table of Contents:

1. Abstract

This investigation focuses on the velocity dynamics of neutral interstellar hydrogen gas in the Milky Way Galaxy, based on its emissions in the radio spectrum. It is expected that orbital velocity should decrease with distance from the centre.

A 12-metre internet-controllable radio telescope was used to measure Doppler shifts in the frequency of the 21-centimetre spectral line. The recessional velocity of radio sources in the first quadrant of the galaxy was recorded. Based on known values for the Sun's position in the Milky Way, the orbital velocity of radio sources is inferred and plotted against distance from the Galactic Centre.

The results of this investigation reveal the orbital velocity stabilising past a radius of 4 kiloparsecs, within a range of approximately 200-240 km/s, which is strongly inconsistent with the Keplerian hypothesis. This discrepancy could possibly be explained by the presence of unobservable "dark matter" that interacts gravitationally with luminous matter.

2. Introduction

2.1 The History of Radio Astronomy

Astronomy is commonly regarded as the oldest of the natural sciences. Humankind's innate fascination with the night sky is responsible for a significant proportion of scientific discoveries. On a dark night, the sky reveals thousands of stars, and the dusty band of the Milky Way Galaxy.

Ever since the invention of the first optical instruments, astronomers have carefully studied the visible universe, through the few wavelengths of light that human eyes can detect. Other parts of the electromagnetic spectrum have been discovered since the 19th century, owing to the works of William Herschel and James Clerk Maxwell. The latter, a renowned Scottish physicist, was able to piece together light and electromagnetism, predicting the existence of radio waves.

While visible light allowed us to observe stars and ionised gas surrounding them, the interstellar medium, made up of cold gas and dust, remained invisible. That is, until the birth of radio astronomy.

Before the 1930s, astronomers had never thought to study the universe outside the visible spectrum. The beginning of radio astronomy was almost accidental. In 1932, engineer Karl Jansky detected a source of noise affecting radio communications. After months of tracking, Jansky determined that this source was not moving relative to distant stars (Jansky, 1933). The source of this mysterious signal was, in fact, the centre of our galaxy.

Galaxies, including our own, are vast systems containing stars, dust, and gas, all of which are gravitationally bound together. Galileo Galilei was the first to resolve the Milky Way into countless stars, in 1610, marking a turning point in our understanding of the universe. The Milky Way has a disk-shaped structure, featuring spiral arms where new stars form, and a dense central region commonly known as the "bulge."

Our position inside the Milky Way galaxy's disk makes it extremely difficult to observe sources behind the centre. This is because light is absorbed by matter in its path, attenuating its intensity before reaching Earth. However, longer wavelengths of light, such as radio, are not affected as much (Liu & Chronopoulos, 2008). Furthermore, Earth's atmosphere does not absorb radio waves, which permits accurate, high-resolution measurements from ground telescopes. Thus, the discovery of extrasolar radio signals was pivotal to the understanding of our Galaxy, leading to the publication of the first sky map at radio frequencies by Grote Reber, in 1943. (NRAO)

2.2 Astronomical Spectroscopy

The electromagnetic spectrum contains spectral lines, regions of stronger or weaker intensity caused by the emission or absorption of a particular frequency of light.

When a photon of light with a particular frequency strikes an atom, it is absorbed, exciting an electron to a higher energy level. After a random amount of time, this electron will de-excite to a lower energy level, releasing energy in the form of light. Thus, an emission line will appear on the electromagnetic spectrum. The discrete frequencies at which this phenomenon can occur are innate to each element.

Spectral lines have many applications in astronomy, from determining the composition of celestial objects to measuring the velocity of distant objects through the Doppler effect. After learning of Reber's accomplishment, Dutch astronomer Jan Oort realised the importance of discovering a spectral line at radio wavelengths. He expected that a radio frequency spectral line would allow us to study the concentration and dynamics of cold interstellar gas with unprecedented accuracy.

In 1945, his student Hendrik van der Hulst published a paper suggesting the possibility of a "hyperfine spectral line of neutral interstellar hydrogen" existing at a wavelength of 21 centimetres. Despite initial scepticism in the scientific community, this line was eventually detected by Harold Ewen and Edward

Purcell in 1951, at Harvard University, using a specialised “horn” radio antenna known as a radiometer. Given the abundance of hydrogen in the interstellar medium, the 21-cm line would prove itself instrumental to a generation of astrophysicists. (NRAO)

2.3 The Doppler Effect

One crucial application of the hydrogen line is the study of velocity dynamics of interstellar gas, via the Doppler effect. The Doppler effect describes the change in frequency observed when a light source is in motion.

If a source is moving away from us, its wavefronts spread out, decreasing the frequency of emission. This phenomenon is called redshift, as visible light would shift towards the red end of the spectrum. The opposite effect occurs when a source is moving towards us, causing blueshift.

Since the spectral line patterns of different elements are unique and well-known, we can identify the spectrum, and compare the observed positions of spectral lines to the expected spectra of a non-moving source, thus determining the Doppler shift and its associated radial velocity.

Each spectral line has a “line width.” The broadening of a spectral line is related to the lifetime of the excited state. (Giuliani, 2005). The 21-cm hydrogen line is particularly narrow, which means it covers an extremely small range of frequencies, making Doppler shift measurements using this line extremely precise. Thus, the observation of radio-emitting neutral hydrogen has provided considerable insight into the velocity dynamics of our galaxy and allowed us to map its rotation pattern.

2.4 The Dynamics of Galactic Rotation

All cosmic objects rotate, including planets, stars, and the gas and dust in our galaxy, due to the conservation of angular momentum since the inception of our universe. During the evolution of a spiral

galaxy, the random rotation and motion of gas and dust stabilised to a single plane of average rotation, forming the galactic disk. Our sun, like most stars in the galaxy, orbits the centre of the galaxy in the same plane.

In Newtonian mechanics, orbital velocity is related to the mass inside the orbit. Analysing rotational velocity and the trajectories that stars and gas clouds follow can elucidate the mass distribution and gravitational fields present in our galaxy. The relationship between distance from the centre and rotational velocity is particularly useful, as it reveals the mass density at different radii. Studies of this relationship involve graphs of Velocity against Radius, or V(R), called rotation curves. (Bertone & Hooper, 2018)

This investigation aims to establish a rotation curve for the Milky Way, following in the footsteps of the great astronomers of the 20th century, to verify whether the orbital dynamics of our galaxy are in concordance with a Keplerian model where most of the mass is concentrated towards the central bulge.

3. Research Review

The first step of this investigation is to establish a comprehensive review of the fundamental principles at the base of 21-cm hydrogen observation: the hydrogen spectrum itself.

3.1 The Hydrogen Spectrum

The electron in a hydrogen atom can occupy discrete energy levels, described by an integer n. The ground state, or the lowest energy level possible, is at n=1. In theory, there can exist an infinite amount of energy levels, up to $n = \infty$, which represents an electron that has been ionised.

However, electrons at very high energy levels become exponentially close to the ionisation energy, and are very weakly bound to the proton, and thus can be removed by any slight disturbance. In practice, only

emissions caused by de-excitation between the first few energy levels are commonly detected as spectral lines, as the others are far too rare to produce a significant signal. Only four spectral lines lie within the visible spectrum.

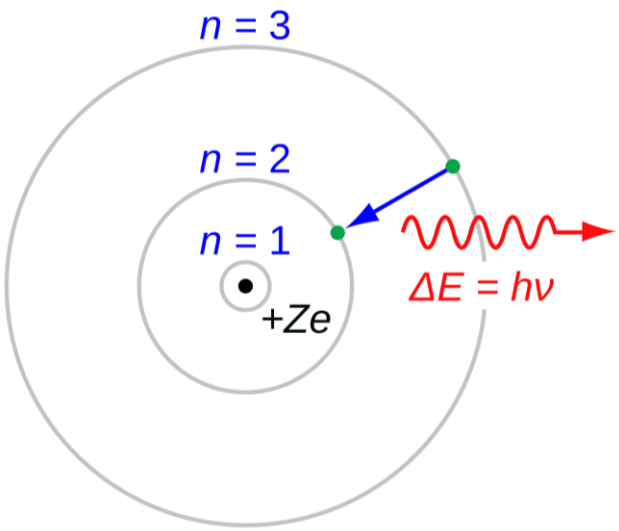

Figure 1 - The emission of a visible spectral line from a hydrogen atom.

Credit: JabberWok, CC BY-SA 3.0 <http://creativecommons.org/licenses/by-sa/3.0/> , via Wikimedia Commons

However, the ground state of hydrogen, n=1, is actually divided into two sublevels, due to the two configurations in which the nucleus and electron spin occur, which can be either parallel or antiparallel. The latter state is slightly excited and thus more energetic. (Giuliani, 2005)

An exchange between these two sublevels is possible, where an electron can “flip” to the antiparallel state, releasing a small amount of energy in the form of radio waves. The wavelength of this emission is precisely 21.1061141 cm (Hellwig et al, 1970).

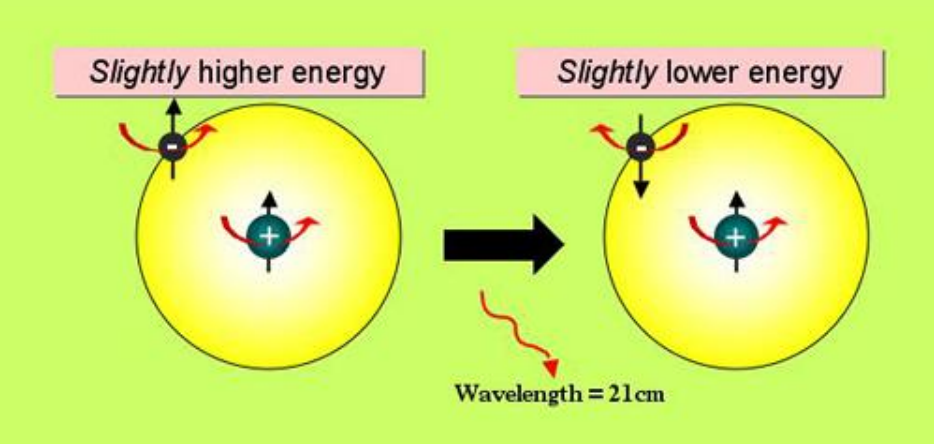

Figure 2 - The spin-flip transition

Credit: © Swinburne University of Technology

Link

The probability of this occurrence is incredibly small, as electrons exist at the upper sublevel for approximately 11 million years. This lifetime results in an exceedingly small line width, allowing for precise Doppler shift measurements (Giuliani, 2005).

3.2 How do Radio Telescopes work?

Radio telescopes are made of two parts: an antenna, and a motor mount. Due to the long wavelengths of radio waves, and their faint nature, telescope antennas must be exceptionally large, often more than 10 m in diameter. The telescope used for this investigation has an antenna 12.2m in diameter.

The parabolic antenna is meant to “collect” and focus radio waves to a focal point (Figure 3), much like an optical reflector telescope would. Radio waves cause the oscillation of free electrons in metals, which can be converted into an electrical signal. Once the radio waves are focused, they are detected and amplified by special receivers, which are custom-built for specific frequency ranges of observation, such as the neutral hydrogen emission line.

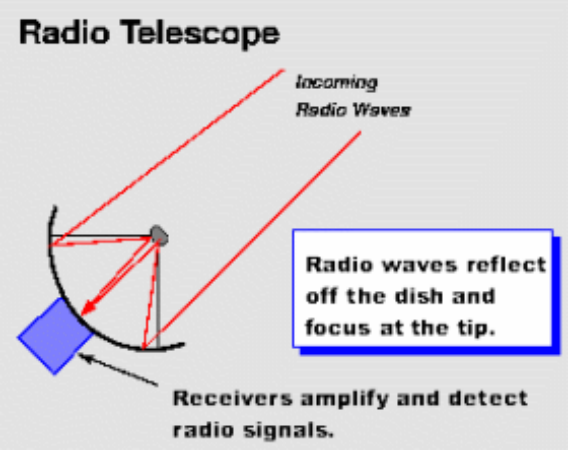

Figure 3 - The basic structure of a radio telescope antenna

Credit: © 2023 The National Radio Astronomy Observatory

Link

The observed frequency range is divided by computers into many separate channels, and the signal intensity is determined for each channel. This is how telescopes are able to measure Doppler shifts in the 21-cm hydrogen line.

3.3 Doppler Effect Conventions

In order to calculate the relative velocity of a light source, the detected frequency shift must be input in the Doppler formula. The most accurate expression of the Doppler Effect for light considers relativistic time dilation (Figure 4) This means that time is dependent on the observer and may appear to dilate or contract depending on the observer's velocity, such that the speed of light remains constant.

Doppler effect for light

$$\nu_{observed} = \left[\frac{\sqrt{1-\frac{v^2}{c^2}}}{1-\frac{v}{c}}\right]\nu_{source}$$

which can be rearranged to the form

$$\nu_{observed} = \nu_{source}\sqrt{\frac{1+\frac{v}{c}}{1-\frac{v}{c}}}$$

Figure 4 - The Relativistic Doppler effect for light

Credit: Relativistic Doppler Shift - HyperPhysics (©C.R. Nave, 2017) - Georgia State University

However, when dealing with velocities that are insignificant compared to the speed of light, the Doppler formula can be approximated for non-relativistic velocities, by taking time as independent to the observer. In this investigation, the relative velocities calculated are rather negligible compared to the speed of light, and any error caused by the non-relativistic approximation can be ignored. There are two conventions in astronomy for carrying out this approximation, as shown below:

$$V_{optical} = c\frac{\lambda_{obs} - \lambda_{rest}}{\lambda_{rest}} \qquad V_{radio} = c\frac{\nu_{rest} - \nu_{obs}}{\nu_{rest}}$$

Figure 5 - Conventions for the non-relativistic Doppler effect: Optical (left), Radio (right)
Credit: National Radio Astronomy Observatory - Guide to Observing with the VLA - Spectral Line
Link

The optical convention (shown to the left) is commonly used for optical measurements in the visible spectrum, as most of these measurements are based on wavelength. However, radio telescopes typically measure frequency shifts rather than wavelengths, and thus the radio convention is used. In Figure 5, the Greek letter ν (nu) is used to denote frequency. The Radio convention formula will be used for all aspects of this investigation.

3.4 Frames of Reference

In astronomy, two types of velocity are commonly measured. Radial velocity is the relative velocity in the line of sight (or direction of observation). Proper velocity is transverse to the line of sight and is often determined by measuring angular displacement. This investigation focuses on the radial velocity component.

The velocities of celestial objects, and objects in general, are always within a frame of reference. On Earth, we commonly refer to the Earth's surface at our position as a frame of reference. This is called a topocentric frame of reference. However, when studying objects outside our planet or even our solar system, it is much more convenient to measure velocities with respect to the Sun, or the galactic centre. The following frames of reference are used in this paper:

Topocentric - Velocity relative to the observer's position on the surface of Earth

Geocentric - Velocity relative to the centre of Earth

Heliocentric - Velocity relative to the Sun

Local Standard of Rest - Velocity relative to the orbit of the local group of stars

Galactocentric - Velocity relative to the Galactic Centre

There are other commonly used frames of reference, such as the Milky Way's local cluster of galaxies, but these are not necessary for this investigation.

The Doppler frequency shifts measured by the telescope are in the topocentric frame of reference. Therefore, the relative velocity output will include the components of Earth's rotation and revolution, in the direction of observation, as illustrated in Figure 6. Therefore, the observed recessional velocity must be corrected for the Earth's rotation and revolution.

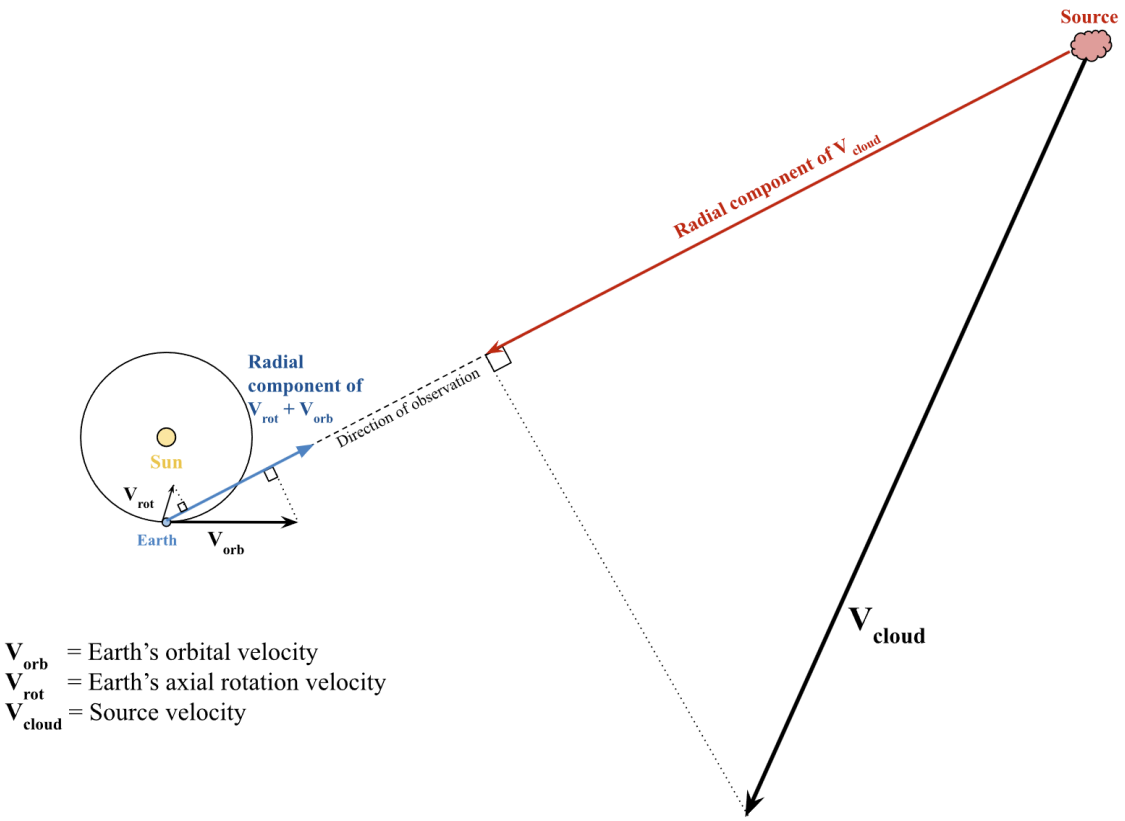

Figure 6 - The radial components of Earth and the Source's velocities.

Note that distances are not to scale, and that the Earth's orbit is incredibly small compared to the source distance, and thus can be ignored. The Earth's orbit is only shown for illustrative purposes. In practice, the heliocentric and geocentric frames of reference are treated as having the same position, while in motion relative to each other, and galactic observations are often assumed to be made from the Sun's position. (Carroll & Ostlie, 2007)

Earth orbits the Sun at an average velocity of 29.8 km/s while rotating around its axis at up to 0.47km/s (Williams, D. R., 2023), depending on the latitude. Once both of these velocities have been corrected for, the relative velocity is said to be in the heliocentric frame of reference.

Furthermore, the relative velocity must be corrected for another component in the line of sight, caused by the Sun's motion relative to the Local Standard of Rest (LSR). The Sun does not follow a perfectly circular orbit, and it is much more useful to refer velocities to the circular orbit of the Local Standard of Rest , based on the average motion of local stars. The Sun's velocity relative to the LSR is called peculiar motion. It has been estimated at about 20 km/s in the direction of the solar apex, towards approximately RA=18 hours, Dec=30 degrees.

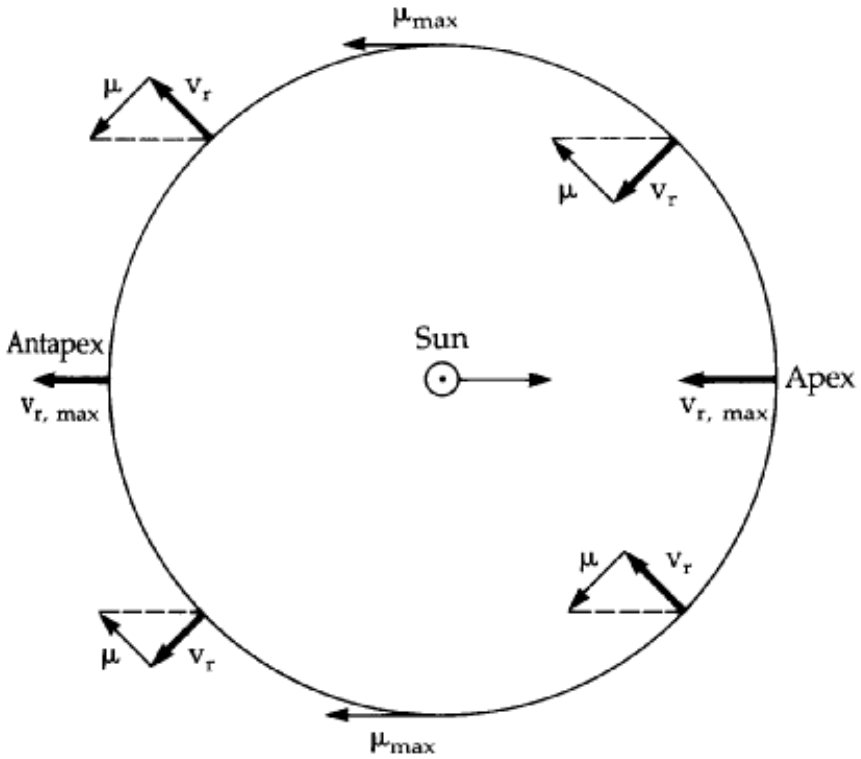

Figure 7 - The apparent relative motion of local stars due to the Sun's peculiar motion.

Credit: Solar Motion. Case Western Reserve University (2023). Notes for the course Str222. Retrieved from http://burro.case.edu/Academics/Astr222/Galaxy/Kinematics/solarmotion.html

The coordinate systems and geometric calculations used to determine orbital velocity are described in the Experimental Methods section.

3.5 The Galactic Constants

Throughout the experimental method, there are two key parameters that need to be applied: the Sun's orbital radius, and as previously discussed, the Local Standard of Rest (LSR) velocity. It is important to understand the way that they are calculated. They are difficult to determine accurately, due to our unfavourable position in the Milky Way's disk. Optical light is affected by considerable extinction due to galactic dust, and radio measurements may be affected by significant local velocity dispersion. Some of the most advanced methods used to study the galactic constants are explained below.

Astronomers can measure the apparent brightness at optical frequencies of stars with known luminosity properties, such as periodic variable stars with predictable luminosity fluctuations (RR Lyrae and Miras), and red clump stars with a known evolutionary path. The distance to the observed stars can be determined using the inverse square law of light intensity. The main obstacle to this method is the extinction of visible light from the Galactic Centre. Due to our position inside the disk of the Milky Way, gas and dust in our line of sight absorb visible light, reducing the accuracy of brightness measurements. (Clayton, 2013)

Another common method used relies on measuring the annual parallax of large molecular clouds that emit radio waves. As Earth moves in its orbit around the Sun, celestial objects shift very slightly in their apparent position, resulting in parallax (Figure 10). The magnitude of parallax is inversely proportional to the source distance, which can be accurately determined due to the transparency of galactic dust at radio frequencies. However, this method requires an incredibly high resolution to resolve the parallax involved, and even the largest radio interferometers can only measure the Sun's orbital radius with a significant uncertainty. (Clayton, 2013)

One of the most precise measurements made of the distance to the Galactic Centre was made by the GRAVITY collaboration in 2019. Abuter et al., 2019 followed the motion of a star close to the dynamical centre of the galaxy, the supermassive black hole Sagittarius A*. Their collaboration carried out a series of spectroscopic and astrometric measurements to map the star's orbital motion. A distance of $8178 \pm 13_{stat.} \pm 22_{sys}$ pc was determined, which will be used for this investigation.

The Local Standard of Rest velocity is even less certain. Several studies have placed it at values between 184 - 254 km/s (Olling & Merrifield, 1998; Kerr & Lynden-Bell, 1986; Reid et al., 2009). Most of these measurements are based on radio interferometry, where a large array of radio telescopes is used to take Doppler shift measurements of the radio source. The measurements made by each telescope are then compared, and minuscule differences between each telescope can be used to resolve slight changes in position and velocity across the Galactic Centre.

The International Astronomical Union (IAU) adopted the recommended value of 220 km/s in 1985. (Kerr & Lynden-Bell, 1986). Despite the publication of recent studies suggesting higher values for LSR velocity (Honma et al., 2012), and with more accurate results (Mroz et al., 2018), there are still large discrepancies between individual studies. For this reason, and for simplicity, the 1985 IAU standard of 220 km/s will be used throughout this investigation.

3.6 Keplerian Mechanics

The understanding of orbital mechanics is critical when studying galactic rotation. The foundation of modern orbital mechanics lies primarily in the works of Johannes Kepler and Isaac Newton. Kepler was the first to empirically determine that the planets follow elliptical orbits, and he described the mechanics of their motion with three laws. Kepler's third law of motion states that the square of the orbital period is directly proportional to the cube of the orbit's semi-major axis ($P^2 \propto a^3$).

Isaac Newton made a very significant contribution to general mechanics through his own three laws of motion. Newton was able to use his laws, and Kepler's third law, to formulate a generalised expression for the universal force of attraction. He discovered that the constant of proportionality in Kepler's third law is related to the masses of the two bodies.

If we consider a simplified, circular model for orbital motion, where P is the orbital period, r is the orbital radius, m is the mass of the orbiting body and M is the much larger mass of the central body, we can express Kepler's Third Law in the following way (Carroll & Ostlie, 2007, pp 32-33):

$$P^2 \propto r^3$$

$$P^2 = kr^3, \text{ Where } k \text{ is a constant.}$$

We can define the orbital period P as the circumference of the orbit divided by the orbital velocity v, and rearrange to obtain the centripetal acceleration v^2/r in terms of r:

$$P = \frac{2\pi r}{v}$$

$$\left(\frac{2\pi r}{v}\right)^2 = kr^3$$

$$\frac{4\pi^2 r^2}{v^2} = kr^3$$

$$\frac{v^2}{4\pi^2 r^2} = \frac{1}{kr^3}$$

$$\frac{v^2}{r} = \frac{4\pi^2}{kr^2}$$

Both sides of the equation are multiplied by the mass of the smaller body m, resulting in mv^2 / r on the left-hand side, which is equal to the centripetal force. In this model, the centripetal force is supplied by gravitation, so F_c is equal to F_g (Carroll & Ostlie, 2007, pp 32-33).

$$\frac{mv^2}{r} = \frac{4\pi^2 m}{kr^2}.$$

$$F_c = F_g = \frac{4\pi^2 m}{kr^2}$$

As shown in the above expression, gravitational force is proportional to the inverse square of the orbital radius. This principle is known as the inverse square law.

According to Newton's third law of motion, "For any action there is an equal and opposite reaction," the gravitational force exerted by m on M must be equal to the opposite force. Therefore, we can rewrite the equation to include this symmetry and group all remaining constants into G, the universal constant of

gravitation. The final result, as shown below, is Newton's Law of Universal Gravitation. (Carroll & Ostlie, 2007, pp 32-33).

$$F_c = F_g = \frac{4\pi^2 M}{k' r^2}$$

$$F_g = \frac{4\pi^2 Mm}{k'' r^2}, \text{ where } k' = \frac{k''}{M} \text{and } k = \frac{k''}{m}$$

$$F_g = G\frac{Mm}{r^2}, \text{ Where } G = \frac{4\pi^2}{k''} \text{ is the universal constant of gravitation.}$$

Furthermore, by equating the centripetal force to the universal gravitation force derived above, we can determine the orbital velocity as a function of the orbital radius and the mass of the main central body, assuming its mass is significantly larger than that of the orbiting body (M >> m).

$$F_{centripetal} = \frac{mv^2}{r}$$
$$F_{gravitational} = G\frac{mM}{r^2}$$
$$F_c = F_g$$
$$\frac{mv^2}{r} = G\frac{mM}{r^2}$$
$$v^2 = \frac{GM}{r}$$
$$v = \sqrt{\frac{GM}{r}}$$
$$Therefore, \ v \propto \sqrt{r}$$

$G = gravitational\ constant$
$M = mass\ of\ main\ body$
$m = mass\ of\ orbiting\ body$
$r = orbital\ radius$
$v = orbital\ velocity$

This demonstrates once again the inverse square law of gravitation. Although Newton was not the first to suggest that the planets in our solar system followed this relationship, he was able to generalise it for any celestial object, and correctly attributed it to a gravitational force of attraction, resulting in his Law of Universal Gravitation. Moreover, Newton was able to re-derive Kepler's third law to apply for any elliptical orbit followed by a celestial body. Its general form remains the most direct way to calculate masses in our solar system and galaxy, to this day.

Throughout this investigation, galactic orbits are approximated as circular, as a more advanced model would be unnecessary for the experimental method used. Observational evidence based on photometric measurements suggests that the Milky Way is made up of a dense central bulge and a disk with an exponentially decreasing luminosity towards greater radii (Liu & Chronopoulos, 2008). According to Valenti et al. (2016), the bulge is expected to have a mass of about 2.0 * 10^10 solar masses up to a radius of about 1.4kpc.

The mass distribution of the galaxy can be mapped by calculating the enclosed masses at different orbital radii, based on the equation derived previously. A significant proportion of the galaxy's mass is expected to lie within the central region, so the rotation curve should show an exponential decay at larger radii, similar to the motion of planets in the Solar System (**Figure 8**).

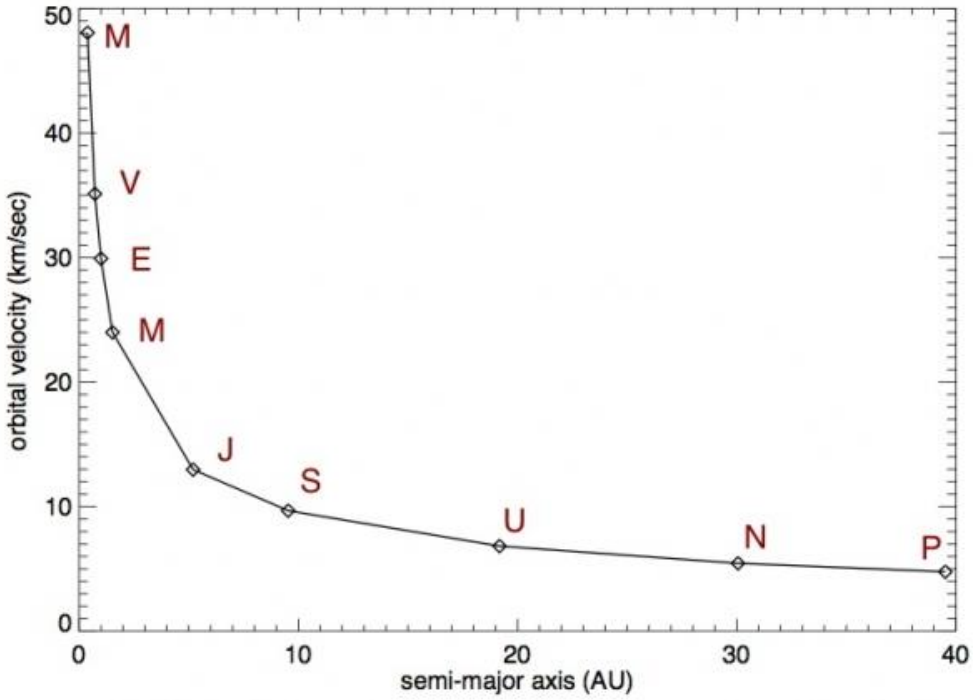

Figure 8 - Graph of the orbital velocity of Solar system planets (and Pluto).

Credit: Chris Palma. The Rotation Curve of the Milky Way. ASTRO 801 Lesson 8 - The Milky Way Galaxy. Penn State University. Retrieved from https://www.e-education.psu.edu/astro801/content/l8_p8.html

In reality, the galactic dynamics are far more complex, but a similar general relationship should be observed.

3.7 Dark Matter Theory

In stark contrast to the Keplerian hypothesis, rotation curves for the Milky Way and many other galaxies have shown that, when plotting orbital velocity against orbital radius, the graph will flatten out rather than decrease, or at most decrease with a much shallower slope than expected.

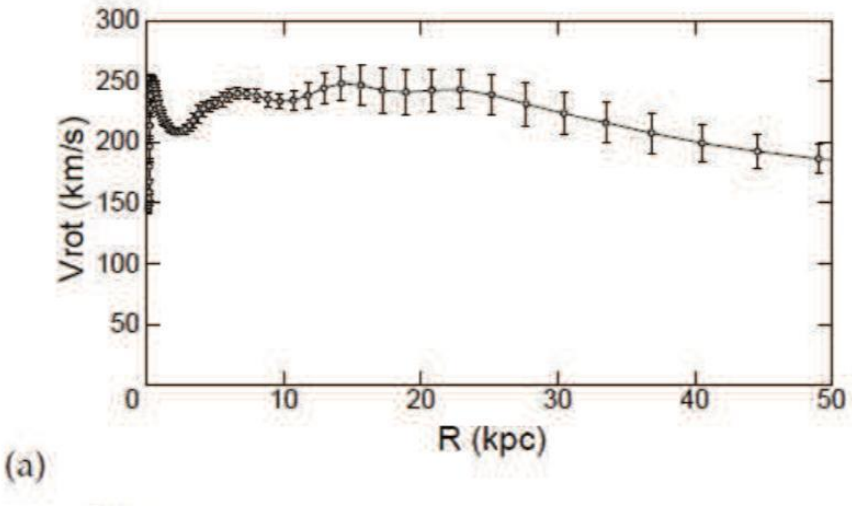

Figure 9: The averaged rotational curve of the Milky Way galaxy in the 0-50 kpc range, based on multiple studies.

Credit: Sofue, 2020.

Link

The visible mass distribution of the galaxy does not correlate to our measurements of galactic rotation, which implies that there may be an undetectable mass interacting gravitationally with the rest of the galaxy and affecting gravitational potential across the whole galaxy.

The idea of an undetectable source of gravitational attraction has been approached ever since the early 20th century, in a study by Knut Lundmark (1930). In the 1970s, after the 21-cm interstellar hydrogen line was first used to measure galactic rotation, Morton Roberts was among the first to suggest the implications of flat rotation curves, while studying the Andromeda Galaxy:

“The rotation curves decline slowly, if at all, at large radii, implying a significant mass density at these large distances. It is unreasonable to expect the last measured point to refer to the ‘edge' of the galaxy, and we must conclude that spiral galaxies must be larger than indicated by the usual photometric measurements.” (Roberts & Whitehurst, 1972; Rots & Roberts, 1973; Bertone & Hooper, 2018)

It is increasingly difficult to determine where exactly a galaxy ends, due to the sparseness of observable light sources at large distances from the galactic centre. This impediment is amplified by our position within the Milky Way disk. However, joint data from the NASA/ESA Hubble Space Telescope and ESA Gaia space observatory was able to measure the galactic mass accurately within 40 kpc at 1.5 trillion solar masses $M_{\odot}$. (ESA, 2019).

This value is much higher than estimated from photometric measurements, and it is widely acknowledged in the scientific community that as much as 90% of the galaxy’s mass is made up of dark matter. A dark matter halo (Figure 10) surrounding the galactic disk and extending to large radii has been proposed to explain the mass distribution. (Strobel, 2022)

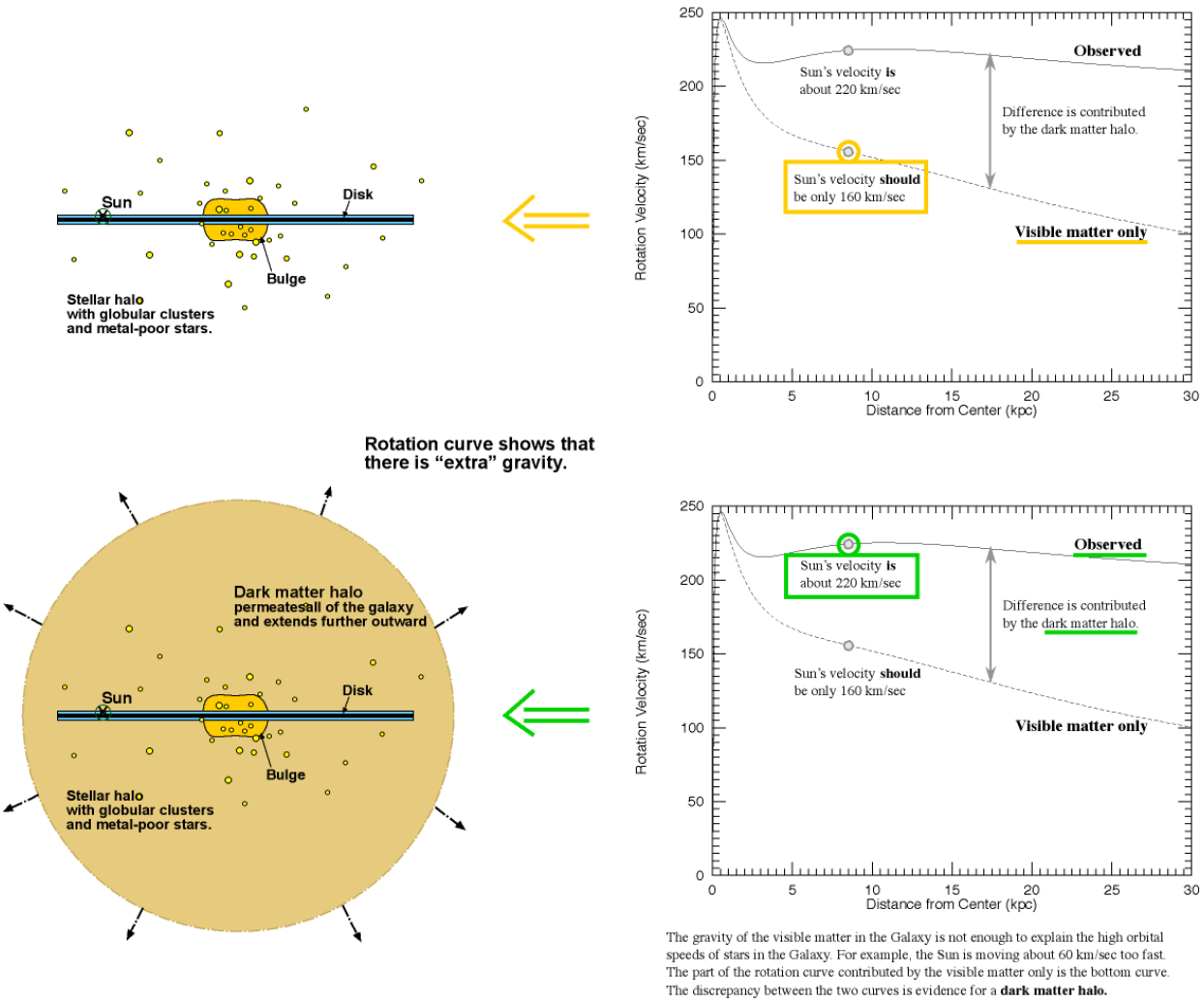

Figure 10: The dark matter halo and its effects on the rotation curve.

Credit: Nick Strobel (2022). Bakersfield College. AstronomyNotes.com. Retrieved from

https://www.astronomynotes.com/ismnotes/s7.htm

3.8 Units, Constants and Definitions

This section includes several defined units and constants used for calculations during the investigation, as well as the definitions of specialised terminology that are referred to in the next stages of this paper.

Table 1:

Name and SI units	Value	Source
Speed of light (vacuum) / ms^{-1}	*299 792 458*	IAU 2009/2012 System of Astronomical Constants
Astronomical Unit (AU) / *m*	*149 597 870 700*	
Constant of gravitation / $m^3\,kg^{-1}\,s^{-2}$	$6.674\,28 \times 10^{-11}$	
Mass of the Sun ($M_\odot$) / kg	1.988×10^{30}	
1 Parsec (pc) to metre conversion	$3.085\,677\,581 \times 10^{16}$	NASA (general definition in use based on the AU)
1 Light-year (ly) to metre conversion	$9.460\,528\,412 \times 10^{15}$	IAU 2009 (based on the speed of light constant)
[H I] Spectral line frequency / *Hz*	*1 420 405 751.768*	Hellwig, H. et al, 1970
[H I] Spectral line wavelength / m	*0.211 061 141*	
Distance from the galactic centre / pc	$8178 \pm 13_{stat.} \pm 22_{sys}$	Abuter, R. et al, 2019
Local Standard of Rest velocity / ms^{-1}	*220 000*	Multiple sources, explained in Research Review

Definitions:

Spectral Flux Intensity - the intensity of radiation at a specific wavelength from an astronomical source, has unit W/m^2 per Hz (or Jansky)

Degree - An angular unit of measurement in which a full turn/rotation around the origin is 360 degrees.

Arc minute - 1/60th of a degree

Arc second - 1/60th of an arcminute (1/3600th of a degree)

Angular distance - The angle of apparent separation between two lines of sight, from the position of an observer.

Equinox - One of two events throughout the year when the Sun appears to cross the celestial equator.

Ecliptic - The circle that the Sun appears to trace in the celestial sphere, as the Earth revolves in its orbit.

Meridian - Any one circle, in the celestial sphere, which passes through the Equatorial North and South poles.

Zenith - The point in the celestial sphere directly overhead the observer's position.

Nadir - The point opposite to the Zenith in the celestial sphere, or the topocentric south pole.

Light-year - The distance that light (in vacuum) travels in one year.

Astronomical Unit - The mean distance between the Earth and the Sun throughout the year.

Parsec - The distance at which one Astronomical Unit subtends 1 arc second in the sky.

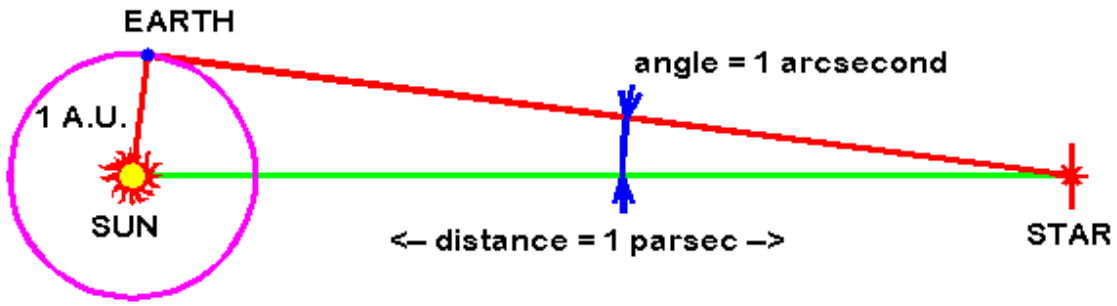

Figure 11 - Stellar parallax and the definition of a Parsec

Credit: Astronomy Stack Exchange, 2013. Original file from Cosmic Reference Guide (Caltech) no longer available online

Link

4. Instrumentation

4.1 Pisgah Astronomical Research Institute

"Pisgah Astronomical Research Institute (also referred to as PARI) is a not-for-profit public foundation located at a former National Aeronautics and Space Administration (NASA) Tracking Station in Western

North Carolina, United States. PARI is a radio and optical observatory engaged in education, research, and public outreach. The 200-acre campus facilities include two 26m radio telescopes, a 4.6m radio telescope, a 12.2m radio telescope, several optical telescopes, and lab space available to researchers and science educators." (Cline, 2006)

In 1963, the Rosman Tracking Station (now known as PARI), was opened by NASA. The station was used for satellite telecommunications and foreign satellite surveillance by the Department of Defense during the Cold War. In 1997, it was purchased by Donald and Jo Cline, and became the astronomical research institute it is today.

4.2 The 12-metre Radio Telescope

The 12-metre Radio Telescope at PARI (Figure 12) is one of the few internet-controllable radio telescopes in the world. It was built by the US Army in 1960 and has been used by NASA and the United States Department of Defense for satellite communications.

Figure 12 - Two angles of the PARI 12-metre radio telescope, on July 17th, 2023.

Throughout this project, hydrogen spectroscopy measurements were taken using the telescope's 1420 MHz receiver. The 12-metre telescope has a half-power beam width of roughly 1.2 degrees (Cline, D. et al., 2018), which represents the area of sky in which intensities are measured during an observation.

Its online interface (shown below) allows the user to input an observation target's coordinates in either an Equatorial or Horizontal coordinate system. The telescope's motor mount is based on altitude and azimuth, and it can rotate clockwise or counterclockwise, and rotate upwards or downwards. It does not feature equatorial tracking for target coordinates, so long scan durations are not reliable.

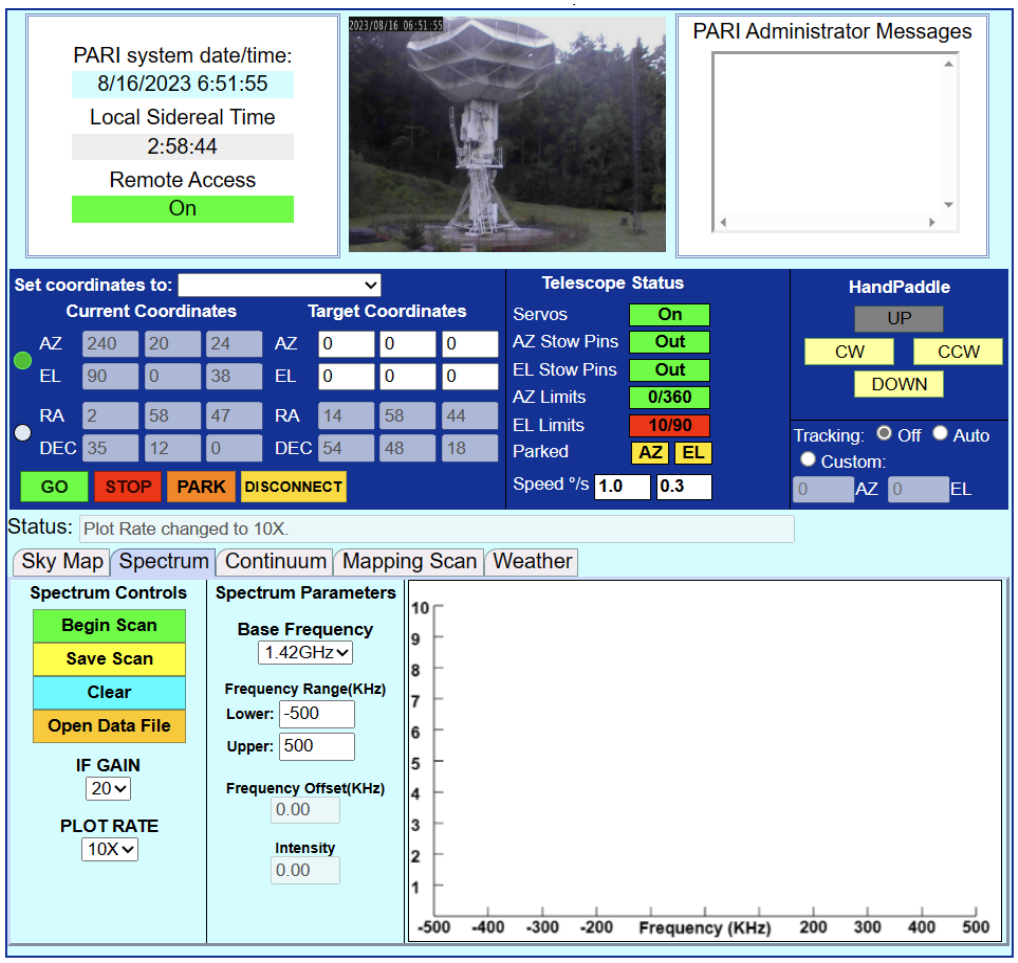

Figure 13 - 12-metre telescope control interface

Screenshot from 12m.pari.edu, login required.

During a Spectrum scan, the telescope spectrometer measures the radiation intensity at Doppler shifted frequencies close to the H I spectral line, within the selected range, defined as the frequency shift (Δf) from the rest value (1420.4 MHz). The online interface outputs the relative intensity and frequency shift for each data point, which is stored as a Flexible Image Transport System (.FITS) file. A graph is also rendered within the interface, with Δf on the horizontal axis, and the relative intensity of radiation on the vertical axis.

For raw data, relative intensity is a unitless quantity. The telescope can be calibrated by observing sources with known intensities, such as the Sun, or Cassiopeia A, and comparing telescope readings with known values. Calibration of the telescope data provides values of spectral flux intensity at each frequency, in Jansky's (power per area per Hz). While this is required for mapping the concentration of gas in our galaxy, for the purposes of this paper calibration is unnecessary.

Lastly, the telescope's safety features include a lightning detector, which shuts the telescope's motors off in the event of a nearby electrical discharge.

5. Experimental Methods

This section of the paper follows a simple process for choosing observation points and calculating their coordinates, as well as the calculations required to convert a Doppler shift into recessional velocity.

5.1 Coordinate systems - Horizontal, Equatorial (and Ecliptic), Galactic

This investigation consists of the observation and spectral analysis of 45 points along the galactic plane.

In order to understand how observation positions are calculated, we must first establish an understanding of the three coordinate systems in use. All three are spherical coordinate systems that represent the projection of the sky visible from Earth, albeit each using different reference planes.

The Horizontal Coordinate System (Figure 14, also known as altitude-azimuth) takes an observer's local horizon as a reference plane. Consequently, the position of an object in this system fluctuates with time, and the observer's latitude and longitude on Earth. Horizontal coordinates are described by the following components:

- Altitude (alt.) represents the angle above or below the horizon. It can take values between -90° and 90°. Only objects with a positive altitude (above the horizon) are visible.

- Azimuth (az.) represents the angular distance from north, in the east direction. It can take values between 0° and 360°. North = 0°, East = 90°, South = 180°, West = 270°

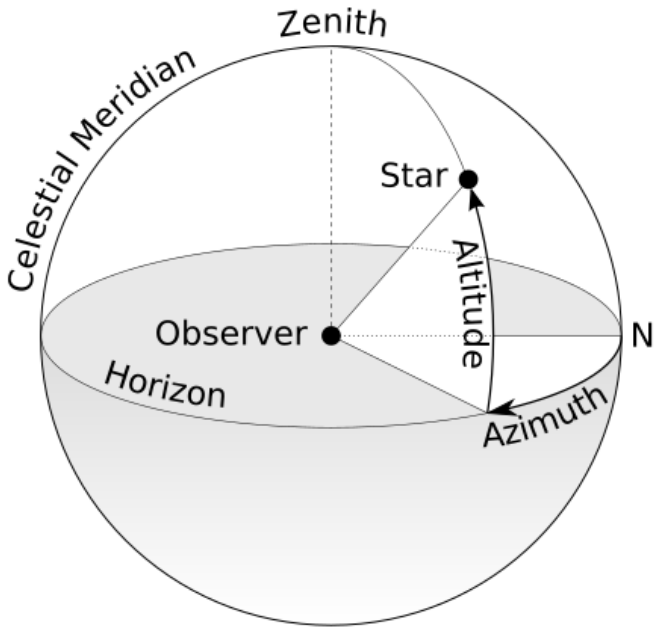

Figure 14 - The Horizontal Coordinate System

Credit:TWCarlson - Wikimedia Commons

Azimut altitude.svg, CC BY-SA 3.0 - Link

The Equatorial Coordinate System, in contrast to the former, takes the Earth's equator as a plane of reference, using the Earth's centre as its origin, and with its poles aligned to the Earth's poles. Equatorial coordinates (measured in Right Ascension and Declination) are the projections of longitude and latitude into a "celestial sphere" with infinite radius.

The Ecliptic line (shown in Figure 16) represents the apparent movement of the Sun throughout the year. It intersects the celestial equator at two points, as the Sun "passes" directly overhead Earth's equator, in events called Equinoxes:

The Spring Equinox occurs during Northern Hemisphere spring, as the Sun crosses the celestial equator and begins to move North. Following this event, days begin to get shorter in the Northern Hemisphere, with the opposite happening in the Southern Hemisphere. The intersection point the Sun appears to cross is called the vernal equinox, shown in Figure 16.

The Fall Equinox occurs during Northern Hemisphere fall, as the Sun crosses the celestial equator and begins to move South. This event is the opposite of the Spring Equinox. This intersection point is called the autumnal equinox.

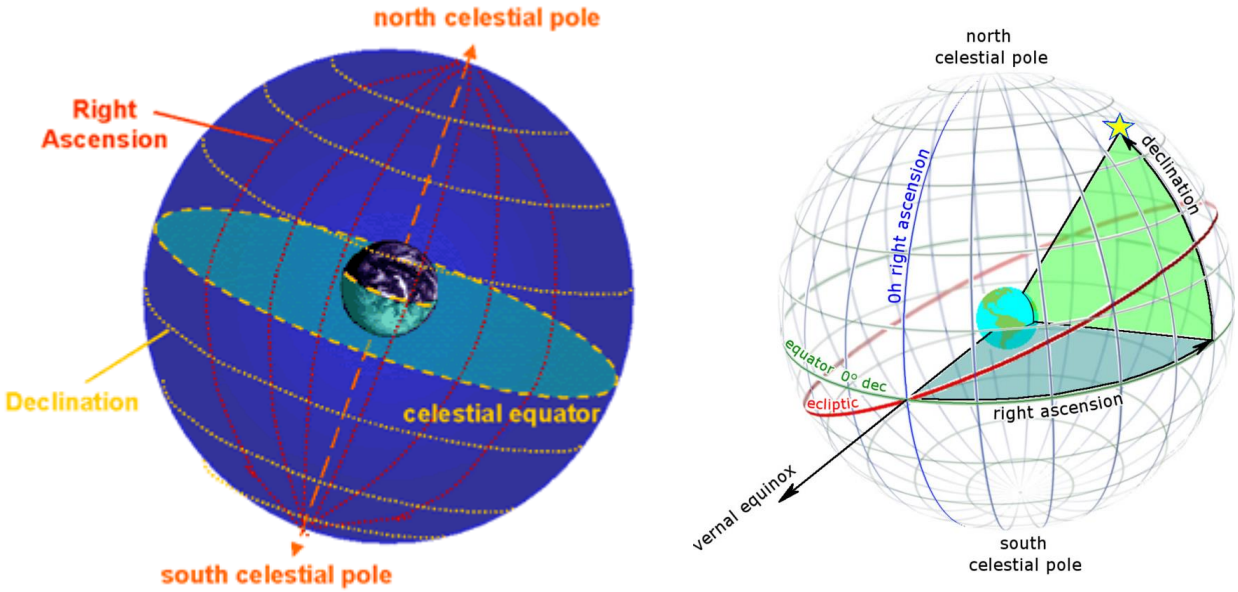

Figure 15 - The Equatorial Celestial Sphere (left)

Credit: Swinburne University of Technology

Link

Figure 16 - Right Ascension, Declination and the Ecliptic (right)

Credit: Wikimedia Commons, Tom Ruen / CC BY-SA 3.0

Link

- Right Ascension (RA) represents the angular distance of an object in the sky from the vernal equinox. As the equivalent of longitude on Earth, it is measured eastward, in hours, minutes, and seconds, such that a full circle is 24 hours. Astronomers established this convention to measure when a star appears to pass the highest point in the sky, crossing the meridian.

- Declination (Dec.) represents how far North or South the object is located in the celestial sphere (the equivalent of latitude on Earth). It is measured in degrees (°), minutes (‘), and seconds (“), where a minute of declination is a 60th of a degree, and a second of declination is a 60th of a minute. The celestial equator has zero declination, whereas the North and South poles have 90° and -90° respectively.

An additional parameter that must be considered is the observation epoch. Over the years, Earth's axis of rotation precesses very slightly with respect to the stars, due to the combined gravitational forces of the Sun and Moon, shifting the position of the north and south celestial poles.
Thus, the equatorial coordinates of an object will change very slightly depending on the date of observation, referred to as the "observation epoch." Astronomers often use RA and Dec coordinates as calculated for Julian year 2000 (Epoch J2000), or during the actual date of measurement, for example, J2023. Throughout this investigation, the J2023 epoch will consistently be used.

For certain calculations, the ecliptic line is used as a reference plane instead of the celestial equator, to simplify equations involving the Sun and planets' positions. This is possible because the Sun and planets all lie in the ecliptic plane, with a "latitude" of approximately zero. This system is called the Ecliptic Coordinate System.

Lastly, the Galactic Coordinate System locates apparent positions in the Milky Way galaxy relative to the galactic centre and the galactic plane. It takes the galactic plane, in which most of the Milky Way's matter is located, as a reference plane, and its origin point is the Sun. An object's position is defined by:

- Longitude (l) is the angular distance from the galactic centre (Shown in Figure 15), measured counter-clockwise in degrees. 0° is the galactic centre, whereas 180° is the anticenter.

- Latitude (b) is the angle above the galactic plane, measured in degrees ranging from -90° (South Galactic Pole) to 90° (North Galactic Pole).

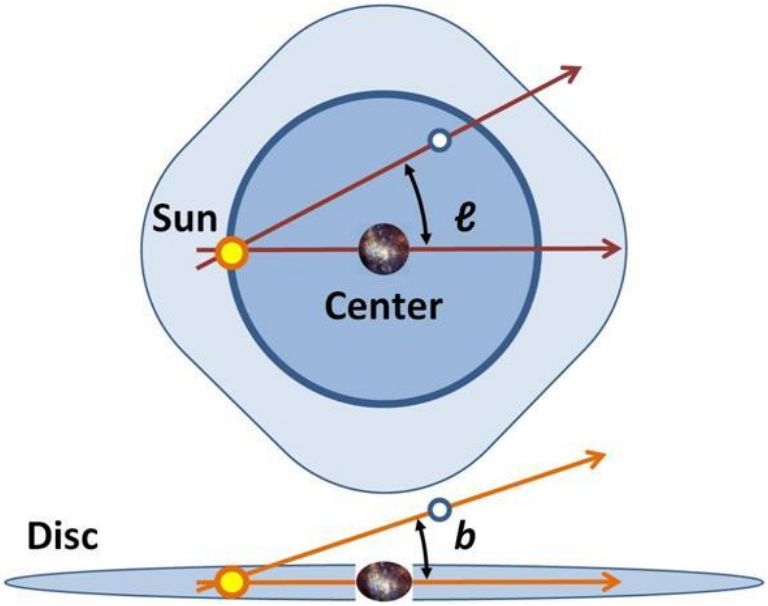

Figure 17 - Galactic coordinates (longitude and latitude)

Credit: Wikimedia Commons, Brews ohare, CC BY-SA 3.0

Link

The positions of the galactic centre and poles were determined following extensive 21-cm hydrogen and optical measurements, and the current system was adopted in 1959 by the International Astronomical Union (Blaauw et al, 1960). This system is particularly useful for estimating the proximity of an object to the galactic centre, thus providing insight into the surrounding mass concentration or rotation speed.

5.2 Tangent-point Method

While galactic coordinates can indicate apparent (angular) distances from the galactic centre with precision, it is not immediately apparent where an object is located along the line of sight. If such an object is interior to the Sun's orbit, we can geometrically determine its orbital radius using the tangent-point method. Therefore, this method only applies to the first and fourth quadrants of the galaxy, between l=0° and l=90°, and between l=270° and l=360°, with a latitude of b=0°.

Outside these ranges, there is no unique orbit that the most red-shifted signal corresponds to (Carroll & Ostlie, 2007). For this investigation, the first quadrant (l=0° and l=90°) is used, as the fourth quadrant is mostly below the northern hemisphere horizon at this time of the year.

The redshift in frequency measured by the 12-metre telescope corresponds to the object's relative velocity in the direction of observation (line of sight). Hence, the most red-shifted signal (largest negative Δf) corresponds to an object whose orbital velocity is entirely in the line of sight. In this case, the line of sight is tangent to its orbit, and perpendicular to its orbital radius, as shown in Figure 16.

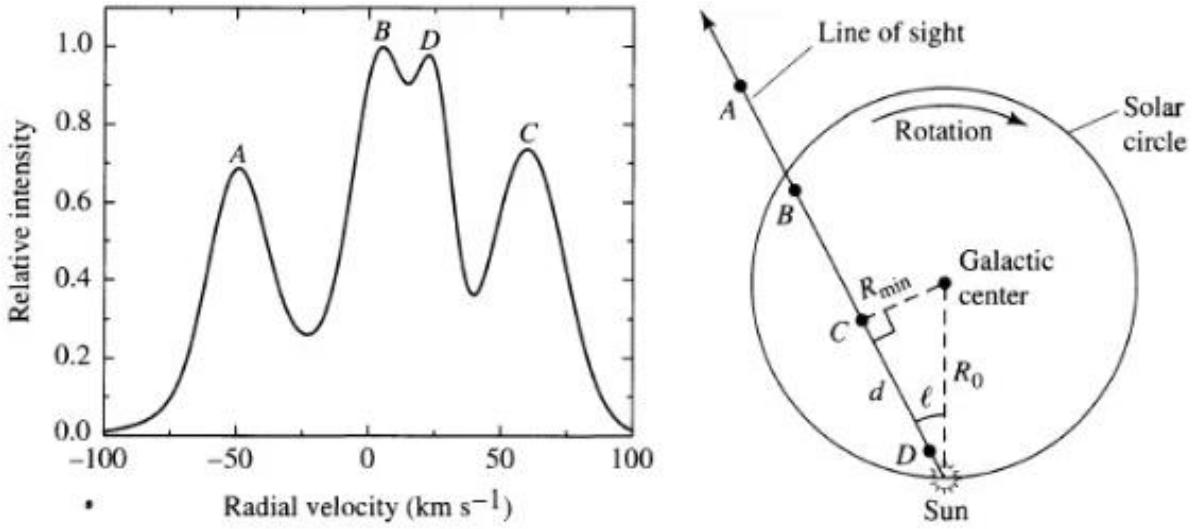

Figure 18 - The spectral profile of H I observation in the line of sight, containing signal peaks from different gas clouds.

Credit: Carroll & Ostlie (2007). Introduction to Modern Astrophysics. p. 914, Fig. 24.24

The distance between the source of maximum redshift and the galactic centre is equal to $R_{min} = R_{\odot} \sin l$.

Therefore, the data collection range (l=0° to l=90°) is divided into 45 observation points, with an interval of 2° in between. The most red-shifted increase in intensity, compared to the noise background, will be recorded for each point. This represents either the most negative frequency shift, where there is a red-shifted signal; or the smallest positive frequency shift in case the entire signal is blue-shifted.

5.3 Coordinate Conversions - NED

The 12-metre radio telescope allows input of equatorial or horizontal coordinates for observation. Galactic coordinates established in the previous section must be converted to equatorial coordinates, which can be input to the telescope's online control interface (Figure 11). The conversion is based on the below formula, where δ is declination, α is right ascension, l is galactic longitude and b is galactic latitude.

$$\sin\delta = \sin\delta_{\mathrm{NGP}}\sin b + \cos\delta_{\mathrm{NGP}}\cos b\cos(\ell_{\mathrm{NCP}} - \ell)$$
$$\cos\delta\sin(\alpha - \alpha_{\mathrm{NGP}}) = \cos b\sin(\ell_{\mathrm{NCP}} - \ell)$$
$$\cos\delta\cos(\alpha - \alpha_{\mathrm{NGP}}) = \cos\delta_{\mathrm{NGP}}\sin b - \sin\delta_{\mathrm{NGP}}\cos b\cos(\ell_{\mathrm{NGP}} - \ell).$$

Figure 19 - Conversion from Galactic to Equatorial coordinates

Credit: Carroll & Ostlie (2007). Introduction to Modern Astrophysics. p. 901, eq. 24.19, 24.20, 24.21

This is a tedious process which is dependent on pre-determined coordinates for the North Galactic (NGP) and Celestial poles (NCP), which are often given in the J2000 epoch, and require additional calculations to be transformed into the J2023 epoch.

For this reason, the NASA/IPAC Extragalactic Database (NED) Coordinate Transformation & Galactic Extinction Calculator is used to convert galactic coordinates to equatorial coordinates for telescope input. A screenshot of the interface is shown below (Figure 20).

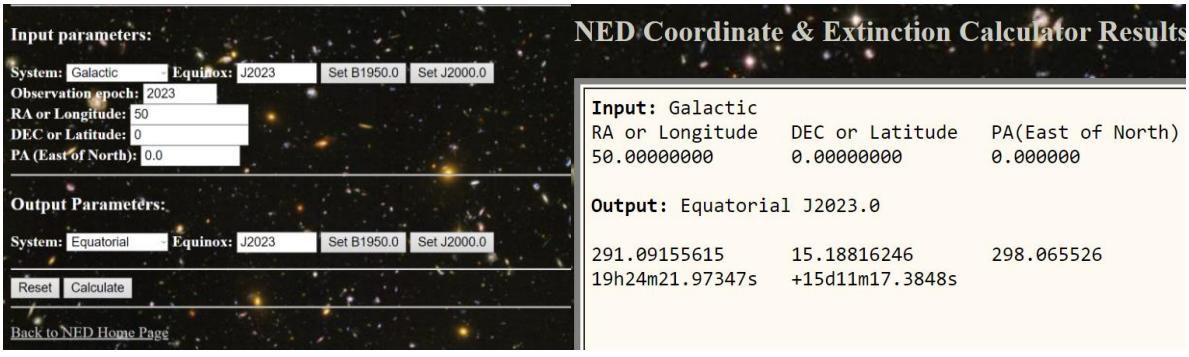

Figure 20 - The Coordinate Transformation calculator interface at https://ned.ipac.caltech.edu/forms/calculator.html

Credit: NASA/IPAC Extragalactic Database Coordinate Transformation & Galactic Extinction Calculator. Hosted by Caltech.

l / °	RA / °	Dec / °	Telescope input (RA Dec)
0	266.7704	-28.94377	17h 47m 05s -28d 56m 38s
2	267.9373	-27.22903	17h 51m 45s -27d 13m 44s
4	269.0686	-25.50490	17h 56m 16s -25d 30m 18s
6	270.1679	-23.77234	18h 00m 40s -23d 46m 20s
8	271.2382	-22.03220	18h 04m 57s -22d 01m 56s
10	272.2825	-20.28528	18h 09m 08s -20d 17m 07s
12	273.3035	-18.53231	18h 13m 13s -18d 31m 56s
14	274.3036	-16.77396	18h 17m 13s -16d 46m 26s
16	275.2854	-15.01088	18h 21m 08s -15d 00m 39s
18	276.2512	-13.24366	18h 25m 00s -13d 14m 37s
20	277.2029	-11.47287	18h 28m 49s -11d 28m 22s
22	278.1428	-9.69904	18h 32m 34s -09d 41m 56s
24	279.0728	-7.92268	18h 36m 17s -07d 55m 21s
26	279.9948	-6.14428	18h 39m 59s -06d 08m 39s
28	280.9106	-4.36431	18h 43m 39s -04d 21m 52s
30	281.8221	-2.58323	18h 47m 17s -02d 34m 59s
32	282.7311	-0.8015	18h 50m 55s -00d 48m 05s
34	283.6393	0.9804	18h 54m 33s +00d 58m 49s
36	284.5484	2.76211	18h 58m 12s +02d 45m 43s
38	285.4603	4.54310	19h 01m 50s +04d 32m 35s
40	286.3766	6.32294	19h 05m 30s +06d 19m 22s
42	287.2993	8.10117	19h 09m 12s +08d 06m 04s
44	288.2302	9.87730	19h 12m 55s +09d 52m 38s

l / °	RA / °	Dec / °	Telescope input (RA Dec)
46	289.1712	11.65086	19h 16m 41s +11d 39m 03s
48	290.1243	13.42132	19h 20m 30s +13d 25m 16s
50	291.0915	15.18816	19h 24m 22s +15d 11m 17s
52	292.0750	16.95079	19h 28m 18s +16d 57m 02s
54	293.0772	18.70861	19h 32m 18s +18d 42m 31s
56	294.1003	20.46100	19h 36m 24s +20d 27m 40s
58	295.1471	22.20725	19h 40m 35s +22d 12m 26s
60	296.2202	23.94665	19h 44m 53s +23d 56m 48s
62	297.3225	25.67839	19h 49m 17s +25d 40m 42s
64	298.4571	27.40162	19h 53m 49s +27d 24m 06s
66	299.6279	29.11537	19h 58m 30s +29d 06m 55s
68	300.8381	30.81862	20h 03m 21s +30d 49m 07s
70	302.0919	32.51022	20h 08m 22s +32d 30m 37s
72	303.3935	34.18890	20h 13m 34s +34d 11m 20s
74	304.7479	35.85328	20h 18m 59s +35d 51m 12s
76	306.1600	37.50181	20h 24m 38s +37d 30m 06s
78	307.6355	39.13277	20h 30m 32s +39d 07m 58s
80	309.1806	40.74425	20h 36m 43s +40d 44m 39s
82	310.8019	42.33411	20h 43m 12s +42d 20m 03s
84	312.5066	43.89995	20h 50m 02s +43d 53m 59s
86	314.3027	45.43908	20h 57m 13s +45d 26m 21s
88	316.1984	46.94851	21h 04m 48s +46d 56m 55s
90	318.2030	48.4248	21h 12m 49s +48d 25m 29s

Table 2 - Table of equatorial coordinates for telescope input

All values given with respect to Julian year 2023 (Epoch J2023.0)

Calculated using https://ned.ipac.caltech.edu/forms/calculator.html

5.4 Observing Schedule - Stellarium

The next step of planning data collection is to determine the best suitable times in which the desired coordinates are in view (above the horizon and tree cover). The 12-metre radio telescope is located in a valley, so tree cover can extend up to about 20° altitude above the horizon. Any data below this altitude is likely affected by significant interference.

Stellarium, a free planetarium software (stellarium.org), is used to estimate the best times for data collection. The longitude and latitude coordinates of the Pisgah Astronomical Research Institute were input into Stellarium, which can produce a realistic view of the visible sky, depending on the time of observation. The galactic coordinate grid (showing longitude lines at intervals of 15°) can be overlaid onto the sky map, showing the apparent movement of the galactic plane in the sky, as Earth rotates around its axis.

For more precise calculations, a star which appears at a short angular distance from the galactic centre is used as a reference. A graph of altitude against local time is plotted, shown in Figure 21. In this case, the highest altitude, of roughly 26°, is reached near 22:00 local time (UTC-4:00). This interval will remain consistent in the following days, and observations near the galactic centre must be conducted around this time.

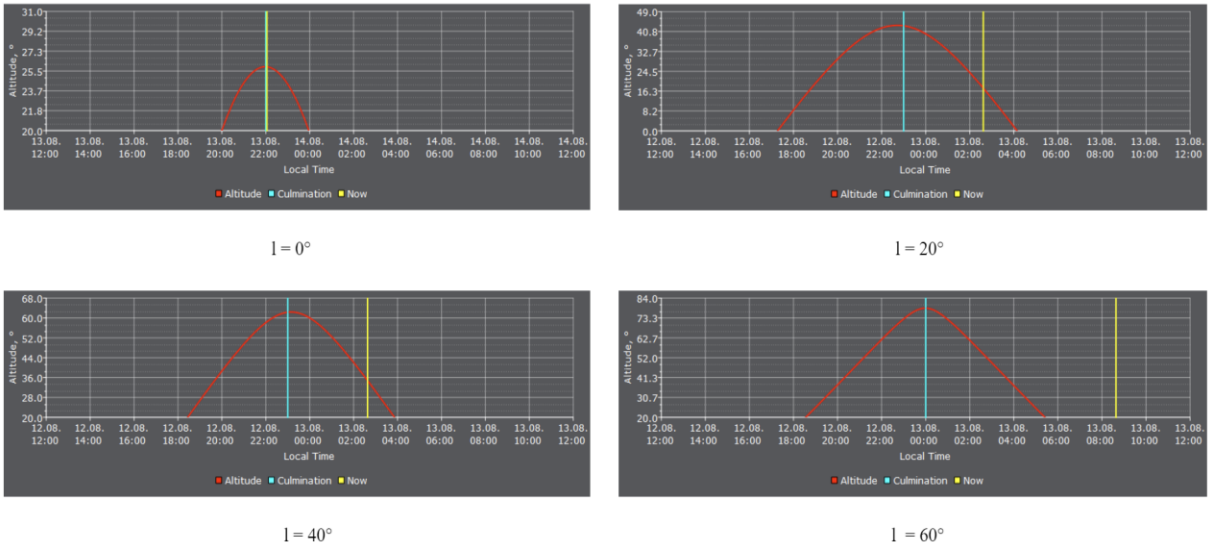

Figure 21 - Graphs of altitude over time for reference stars near galactic longitudes l = 0, 20, 40, 60

Exported from the Stellarium software.

For larger longitudes, the interval in which the object is above tree cover increases to up to 12 hours of visibility, allowing for a more flexible schedule.

A total of five observation sessions were carried out through the course of this investigation, listed below:

Table 3 - Observation schedule:

	Local (telescope) date and time	UTC date and time	Region observed / l°
Session 1	12/08/23 21:30	13/08/23 01:30	00 - 16
Session 2	12/08/23 22:00	13/08/23 02:00	36 - 60
Session 3	13/08/23 07:00	13/08/23 11:00	86 - 90
Session 4	14/08/23 01:30	14/08/23 05:30	62 - 84
Session 5	15/08/23 23:20	16/08/23 03:20	18 - 34

5.5 Data Collection parameters

Frequency ranges in this paper are defined with respect to the 21-cm line rest frequency of 1420.405 MHz. Negative Δf values represent red-shifted (lower frequency) intensities, whereas positive ones represent blue-shifted (higher frequency) intensities. For example, a Δf of -500 KHz represents a frequency of 1419.905 MHz.

For each observing point, a measurement of flux intensity was made every 10 KHz, starting at -500 KHz, until 500 KHz higher than the 21 cm line rest frequency. Points between l =` 18 - 34 contained very red-shifted signals, and thus their scans were redone with a range of (-700 KHz < Δf < +300 KHz), to fit the entire signal width.

Throughout the data collection process, the frequency step between individual measurements was kept constant at 10 KHz, and the telescope's power gain was kept constant at the arbitrary value of 21, to facilitate comparisons between spectrum graphs. However, as previously specified in this paper, calibrating relative intensity into values of spectral flux intensity is unnecessary, as the investigation focuses on changes in frequency rather than intensity.

According to the tangent-point method, the most redshifted (lowest) frequency value must be recorded for each point. This is defined as the first point to have an intensity notably higher than the background noise average. This is taken as any value 5% higher than the noise background for every scan. This is to account for small fluctuations in background noise, or anomalies caused by nearby emission sources on Earth. For example, Figure 22 shows the data collected at l = 44°. The relative intensity of background noise is about 4.90, and therefore the lowest accepted intensity is 1.05 × 4.9 = 5.145. Thus, the most red-shifted signal is taken as -290 KHz.

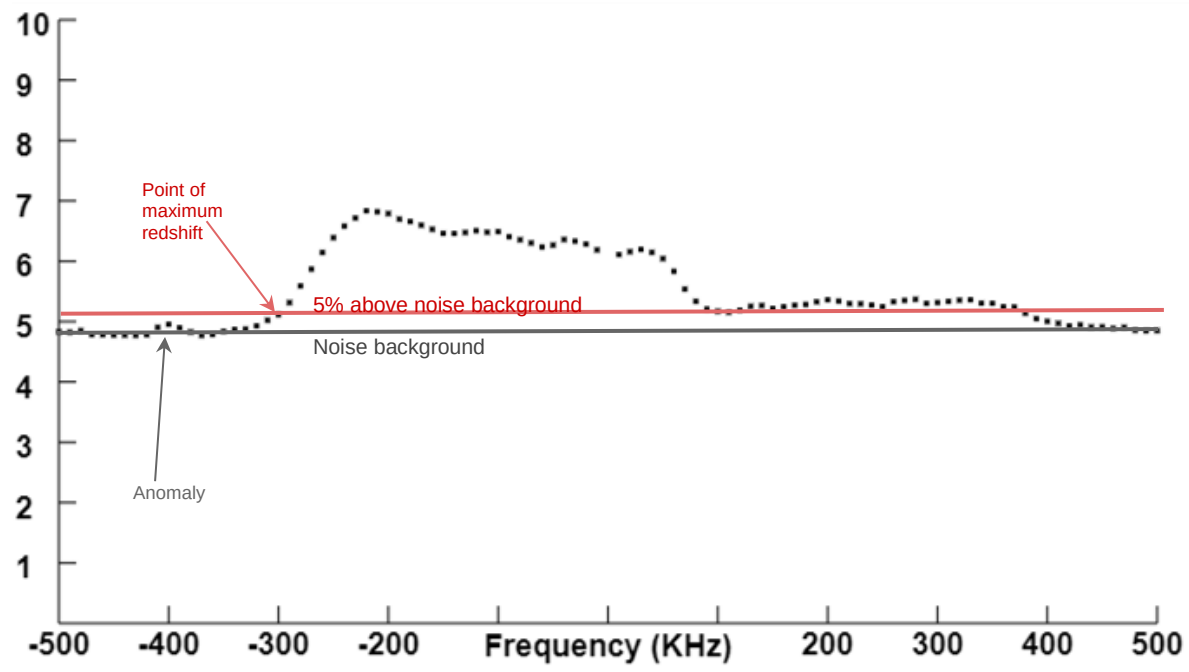

Figure 22 - Scan of l = 44° including noise background and a cutoff line showing minimum significant intensity. The y-axis represents relative flux intensity.

Frequency shift values are taken from the complete .FITS data file, which includes numerical intensity values for each frequency, and entirely eliminates the inaccuracy of a graphical model. The above plot is not used for the actual calculations and is simply meant for a visual representation of the process.

5.6 Doppler Shift Calculations

Once frequency data for each point has been determined, the relative velocity causing the Doppler shift can be identified. Since the relative velocities dealt with (below 300 km/s) are insignificant compared to the speed of light, the relativistic version of the Doppler effect formula is unnecessary, as time dilation does not need to be accounted for
(C. R., Nave). The non-relativistic approximation for the Doppler formula is shown below (Figure 23).

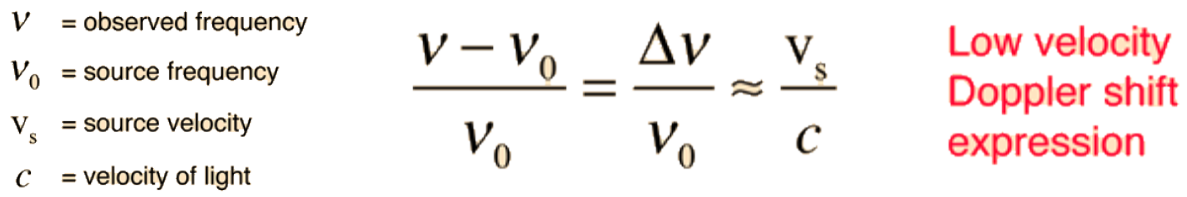

Figure 23 - Low-velocity Doppler shift expression (cropped from original source)

Credit: Low Speed Doppler Shift - HyperPhysics (©C.R. Nave, 2017) - Georgia State University

Link

Therefore, the observed relative velocity is equal to

$$V_r = c\frac{\Delta f}{f_0}$$

Throughout the following calculations, for convenience, observed recessional velocity $V_{obs} = -V_r$ will be used instead of observed relative velocity. A positive V_{obs} refers to an object receding (moving away from us), whereas a negative value for V_{obs} signifies an object moving towards us.

5.7 Adjusting to the Local Standard of Rest

The calculated recessional velocities are with respect to the telescope's topocentric frame of reference. In order to calculate the orbital velocity of radio sources, the radial velocity readings must first be converted to the Local Standard of Rest. For all measurements made, the telescope's position was considered to be stationary, and the apparent relative velocity of observed objects was recorded.

However, with respect to the centre of the Galaxy, the telescope is not stationary. Earth rotates around its axis and revolves around the Sun. As mentioned in the Research Review, both of these velocities are vectors that can be resolved to have a component in the line of sight, which must be subtracted from the recessional velocity. The Earth's velocity of revolution of about 30 km/s can be corrected for using the following equation (MIT Junior Lab, 2016):

$$V_{\mathrm{rE}} = 30.0\left[\cos\beta\,\sin\lambda_{\odot}\,\cos\lambda - \cos\beta\,\cos\lambda_{\odot}\,\sin\lambda\right] = 30.0\,\cos\beta\,\sin(\lambda_{\odot} - \lambda)$$

V_{rE} = Earth's recessional velocity in the line of sight.

β = Ecliptic latitude of target

λ = Ecliptic longitude of target

$\lambda_{\odot}$ = Sun's ecliptic longitude (its latitude is always 0).

Following this calculation, the recessional velocity observed is heliocentric (relative to the Sun's centre.) The tangent-point experimental method assumes that the observer's orbit is a circle with an 8.178kpc radius and a velocity of 220 km s^{-1}. (Kerr & Lynden-Bell, 1986). This value is called the Local Standard of Rest velocity. However, the Sun's motion deviates slightly from this assumption. The Sun, and by extension our Solar System, moves towards an "apex" close to RA = 18h (270°), Dec = 30°, relative to the average motion of local stars. This motion can be corrected by using the following equation: (MIT Junior Lab, 2016).

$$V_{\mathrm{r}\odot} = 20.0\left[\cos 270^{\circ}\,\cos 30^{\circ}\,\cos\alpha\,\cos\delta + \sin 270^{\circ}\,\cos 30^{\circ}\,\sin\alpha\,\cos\delta + \sin 30^{\circ}\,\sin\delta\right]\,\mathrm{km/s}.$$

$V_{r\odot}$ = Earth's recessional velocity in the line of sight.

α = Right Ascension of target

δ = Declination of target

Once the above correction is applied, the recessional velocity is in the LSR frame of reference, which means it is at the Sun's position, following the average orbital motion of local stars. This makes all subsequent calculations in this investigation much more accurate to the assumptions made by the tangent-point method.

Carrying out reference frame corrections manually requires several coordinate conversions, between galactic, ecliptic, and equatorial systems, which can be a large source of systematic error if calculated incorrectly. Instead, the U.S. National Radio Astronomy Observatory (NRAO) "radial velocity calculator" is used (**Figure 24**).

Calculate Radial velocities at the GBT

Calculate

UT date	UT time	Right Ascension	Declination	V-Helio	V_LSRK	V_GAL
2023/08/13	11:00:00	318.2030661	48.4248447	-6.510 km/sec	-21.790 km/sec	-238.480 km/sec

This gives the velocity in the direction (RA,Dec) from the point of view of the GBT.
Positive means it is receding from us (redshift); negative, it is approaching (blueshift).

V-Helio is the velocity due to the rotation of the Earth and the motion of the Earth in its orbit around the Sun.

V-LSRK is the velocity referenced to the local standard of rest, in addition to the motions of the Earth.

V-GAL is the velocity referenced to the center of the galaxy.

Measurements within our galaxy are usually referred to the LSR
Measurements of extragalactic objects are usually referred to the Sun (heliocentric or barycentric), or sometimes to the galactic center (V_GAL).

(These calculations apply just as well to the Green Bank 20-meter telescope.)

RA may be either "hh:mm:ss" or decimal degrees.
DEC may be either "dd:mm:ss" or decimal degrees.
UT time may be either "hh:mm:ss" or decimal hours.

Figure 24 - Radial velocity calculator for the Green Bank Telescope.

Credit: National Radio Astronomy Observatory

Link

The calculator is calibrated for the position of the Green Bank Telescope (GBT), which is only 449 kilometres from the Pisgah Astronomical Research Institute, making the corrections sufficiently accurate for this investigation. Any errors resulting from the difference in position are negligible. An example of its accepted input is shown, for a set of RA and Dec coordinates. The UTC observation time and date must also be provided. The calculated V_LSRK represents the apparent recessional velocity caused by the Earth and Sun's motion, and it must be subtracted from V_{obs} to obtain V_{rec} relative to the Local Standard of Rest.

5.8 Determining the Orbital Radius and Velocity

The values for V_{obs} in the previous section which have been corrected for the Sun and Earth's motion will hereafter be referred to as corrected recessional velocity V_{rec}. Once the recessional velocity for every tangent point has been determined and corrected for the Sun and Earth's motion, the orbital velocity and radius of the observed object can be determined, using the geometry shown in Figure 25.

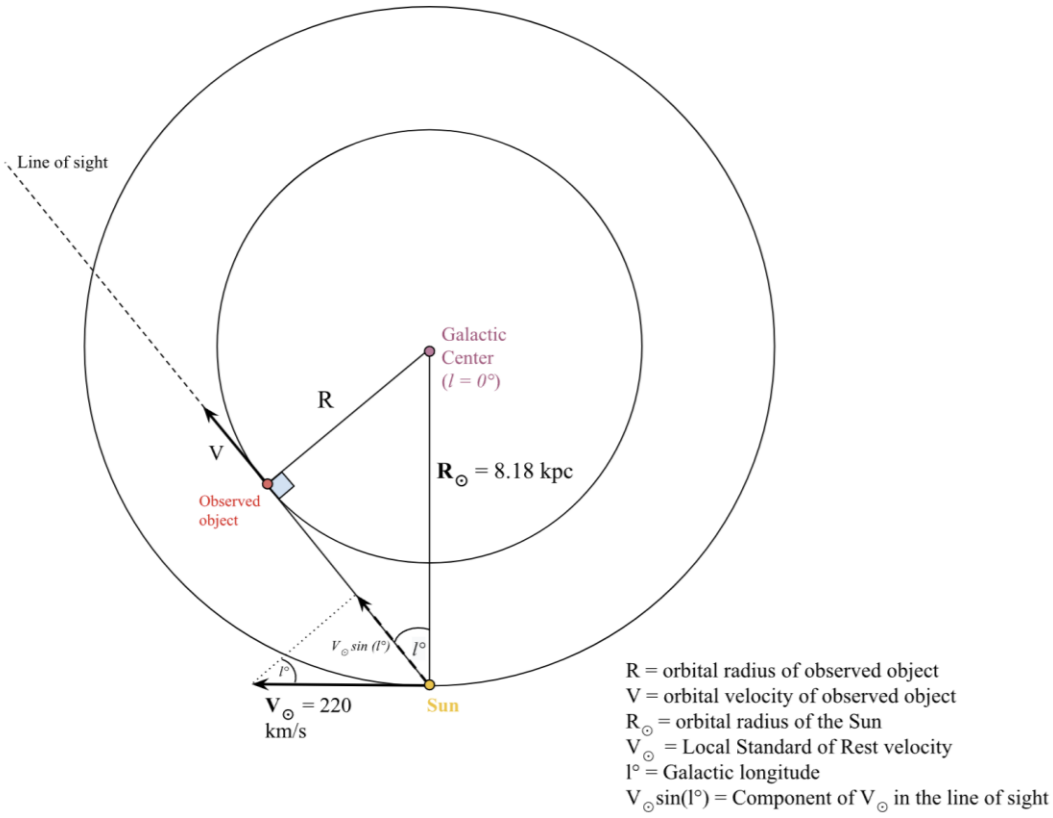

Figure 25 - Geometry used to calculate the orbital radius and velocity of the observed object.

Figure 25 shows the resolution of the vector $V_\odot$ into two perpendicular components. The component of $V_\odot$ in the direction of observation (line of sight) is equal to,

$$V_\odot sin(l)$$

which is added to the corrected recessional velocity V_{rec} to calculate V, the orbital velocity:

$$V = V_{rec} + V_\odot sin(l)$$

Furthermore, the orbital radius is calculated using

$$R = R_\odot sin(l)$$

Due to the shape of the function *sin(x)* between 0° and 90°, recessional velocity near the galactic centre is expected to be relatively similar to the orbital velocity, while near the direction of the Sun's orbit (l=90°) we would expect the recessional velocity observed to be approximately $V - V_\odot$.

6. Data Analysis

6.1 Organising the Data

Microsoft Excel was used to organise experimental data throughout this investigation, and to create some of the graphs shown in the Interpretation section. Figure 26 shows a screen capture of the spreadsheet used.

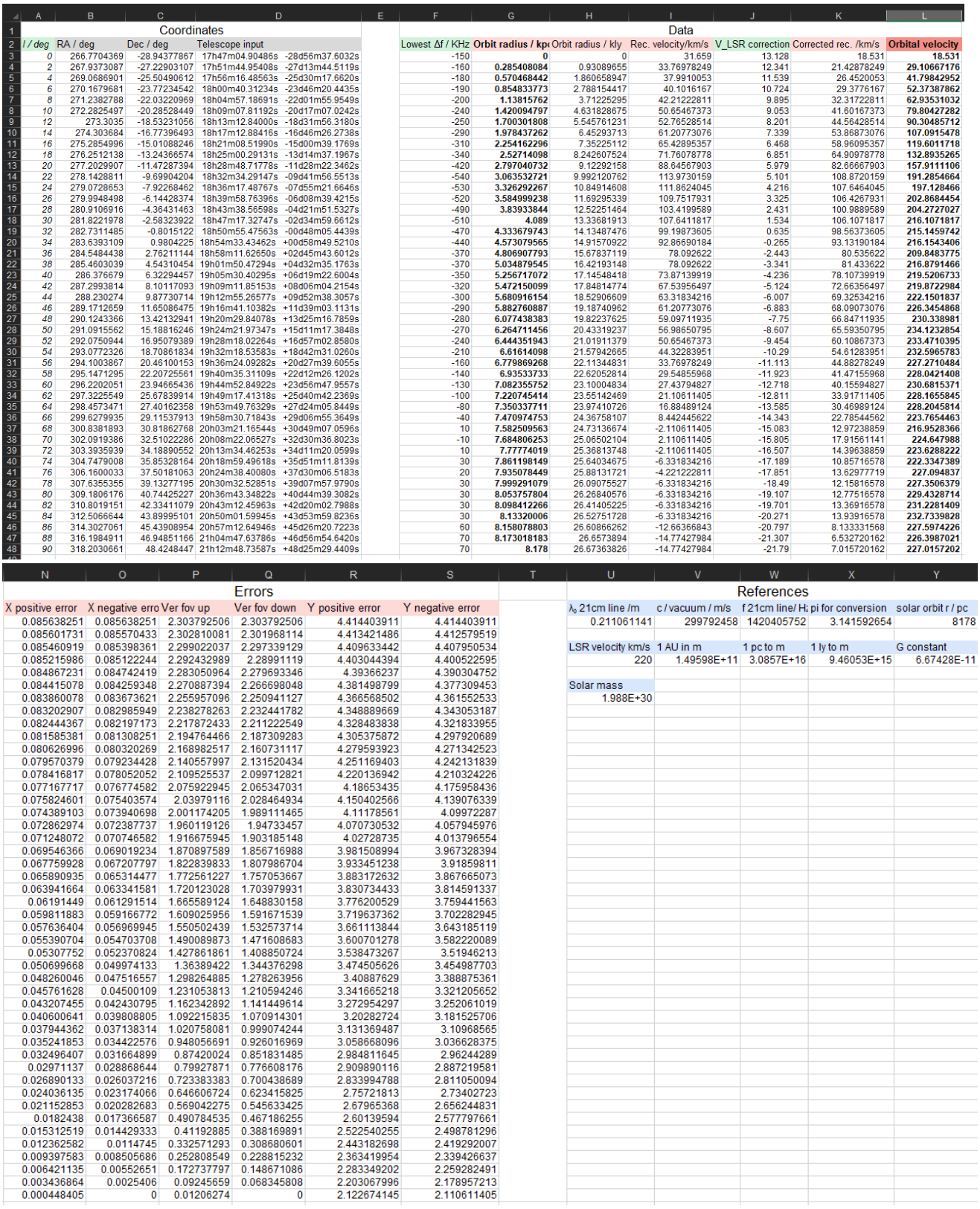

Coordinates				
l / deg	RA / deg	Dec / deg	Telescope input	
0	266.7704369	-28.94377867	17h47m04.90486s	-28d56m37.6032s
2	267.9373087	-27.22903107	17h51m44.95408s	-27d13m44.5119s
4	269.0686901	-25.50490612	17h56m16.48563s	-25d30m17.6620s
6	270.1679681	-23.77234542	18h00m40.31234s	-23d46m20.4435s
8	271.2382788	-22.03220969	18h04m57.18691s	-22d01m55.9549s
10	272.2825497	-20.28528449	18h09m07.81192s	-20d17m07.0242s
12	273.3035	-18.53231056	18h13m12.84000s	-18d31m56.3180s
14	274.303684	-16.77396493	18h17m12.88416s	-16d46m26.2738s
16	275.2854996	-15.01088246	18h21m08.51990s	-15d00m39.1769s
18	276.2512138	-13.24366574	18h25m00.29131s	-13d14m37.1967s
20	277.2029907	-11.47287394	18h28m48.71778s	-11d28m22.3462s
22	278.1428811	-9.69904204	18h32m34.29147s	-09d41m56.5513s
24	279.0728653	-7.92268462	18h36m17.48767s	-07d55m21.6646s
26	279.9948498	-6.14428374	18h39m58.76396s	-06d08m39.4215s
28	280.9106916	-4.36431463	18h43m38.56598s	-04d21m51.5327s
30	281.8221978	-2.58323922	18h47m17.32747s	-02d34m59.6612s
32	282.7311485	-0.8015122	18h50m55.47563s	-00d48m05.4439s
34	283.6393109	0.9804225	18h54m33.43462s	+00d58m49.5210s
36	284.5484438	2.76211144	18h58m11.62650s	+02d45m43.6012s
38	285.4603039	4.54310454	19h01m50.47294s	+04d32m35.1763s
40	286.376679	6.32294457	19h05m30.40295s	+06d19m22.6004s
42	287.2993814	8.10117093	19h09m11.85153s	+08d06m04.2154s
44	288.230274	9.87730714	19h12m55.26577s	+09d52m38.3057s
46	289.1712659	11.65086475	19h16m41.10382s	+11d39m03.1131s
48	290.1243366	13.42132941	19h20m29.84078s	+13d25m16.7859s
50	291.0915562	15.18816246	19h24m21.97347s	+15d11m17.3848s
52	292.0750944	16.95079389	19h28m18.02264s	+16d57m02.8580s
54	293.0772326	18.70861834	19h32m18.53583s	+18d42m31.0260s
56	294.1003867	20.46100153	19h36m24.09282s	+20d27m39.6055s
58	295.1471295	22.20725561	19h40m35.31109s	+22d12m26.1202s
60	296.2202051	23.94665436	19h44m52.84922s	+23d56m47.9557s
62	297.3225549	25.67839914	19h49m17.41318s	+25d40m42.2369s
64	298.4573471	27.40162358	19h53m49.76329s	+27d24m05.8449s
66	299.6279935	29.11537913	19h58m30.71843s	+29d06m55.3649s
68	300.8381893	30.81862768	20h03m21.16544s	+30d49m07.0596s
70	302.0919386	32.51022286	20h08m22.06527s	+32d30m36.8023s
72	303.3935939	34.18890552	20h13m34.46253s	+34d11m20.0599s
74	304.7479008	35.85328164	20h18m59.49618s	+35d51m11.8139s
76	306.1600033	37.50181063	20h24m38.40080s	+37d30m06.5183s
78	307.6355355	39.13277195	20h30m32.52851s	+39d07m57.9790s
80	309.1806176	40.74425227	20h36m43.34822s	+40d44m39.3082s
82	310.8019151	42.33411079	20h43m12.45963s	+42d20m02.7988s
84	312.5066644	43.89995101	20h50m01.59945s	+43d53m59.8236s
86	314.3027061	45.43908954	20h57m12.64946s	+45d26m20.7223s
88	316.1984911	46.94851166	21h04m47.63786s	+46d56m54.6420s
90	318.2030661	48.4248447	21h12m48.73587s	+48d25m29.4409s

Data						
Lowest Δf / KHz	Orbit radius / kpc	Orbit radius / kly	Rec. velocity/km/s	V_LSR correction	Corrected rec. /km/s	Orbital velocity
-150	0	0	31.659	13.128	18.531	18.531
-160	0.285408084	0.93089655	33.76978249	12.341	21.42878249	29.10667176
-180	0.570468442	1.860658947	37.9910053	11.539	26.4520053	41.79842952
-190	0.854833773	2.788154417	40.1016167	10.724	29.3776167	52.37387862
-200	1.13815762	3.71225295	42.212228111	9.895	32.31722811	62.93531032
-240	1.420094797	4.631828675	50.65467373	9.053	41.60167373	79.80427282
-250	1.700301808	5.545761231	52.76528514	8.201	44.56428514	90.30485712
-290	1.978437262	6.45293713	61.20773076	7.339	53.86873076	107.0915478
-310	2.254162296	7.35225112	65.42895357	6.468	58.96095357	119.6011718
-340	2.52714098	8.242607524	71.76078778	6.851	64.90978778	132.8935265
-420	2.797040732	9.12292158	88.64567903	5.979	82.66667903	157.9111106
-540	3.063532721	9.992120762	113.9730159	5.101	108.8720159	191.2854664
-530	3.326292267	10.84914608	111.8624045	4.216	107.6464045	197.128466
-520	3.584999238	11.69295339	109.7517931	3.325	106.4267931	202.8684454
-490	3.83933844	12.52251464	103.4199589	2.431	100.9889589	204.2727027
-510	4.089	13.33681913	107.6411817	1.534	106.1071817	216.1071817
-470	4.333679743	14.13487476	99.19873605	0.635	98.56373605	215.1459742
-440	4.573079565	14.91570922	92.86690184	-0.265	93.13190184	216.1543406
-370	4.806907793	15.67837119	78.092622	-2.443	80.535622	209.8483775
-370	5.034879545	16.42193148	78.092622	-3.341	81.433622	216.8791466
-350	5.256717072	17.14548418	73.87139919	-4.236	78.10739919	219.5206733
-320	5.472150099	17.84814774	67.53956497	-5.124	72.66356497	219.8722984
-300	5.680916154	18.52906609	63.31834216	-6.007	69.32534216	222.1501837
-290	5.882760887	19.18740962	61.20773076	-6.883	68.09073076	226.3454868
-280	6.077438383	19.82237625	59.09711935	-7.75	66.84711935	230.338981
-270	6.264711456	20.43319237	56.98650795	-8.607	65.59350795	234.1232854
-240	6.444351943	21.01911379	50.65467373	-9.454	60.10867373	233.4710395
-210	6.61614098	21.57942665	44.32283951	-10.29	54.61283951	232.5965783
-160	6.779869268	22.11344831	33.76978249	-11.113	44.88278249	227.2710484
-140	6.93533733	22.62052814	29.54855968	-11.923	41.47155968	228.0421408
-130	7.082355752	23.10004834	27.43794827	-12.718	40.15594827	230.6815371
-100	7.220745414	23.55142469	21.10611405	-12.811	33.91711405	228.1655845
-80	7.350337711	23.97410726	16.88489124	-13.585	30.46989124	228.2045814
-40	7.470974753	24.36758107	8.442445622	-14.343	22.78544562	223.7654463
10	7.582509563	24.73136674	-2.110611405	-15.083	12.97238859	216.9528366
-10	7.684806253	25.06502104	2.110611405	-15.805	17.91561141	224.647988
10	7.77774019	25.36813748	-2.110611405	-16.507	14.39638859	223.6288222
30	7.861198149	25.64034675	-6.331834216	-17.189	10.85716578	222.3347389
20	7.935078449	25.88131721	-4.221222811	-17.851	13.62977719	227.094837
30	7.999291079	26.09075527	-6.331834216	-18.49	12.15816578	227.3506379
30	8.053757804	26.26840576	-6.331834216	-19.107	12.77516578	229.4328714
30	8.098412266	26.41405225	-6.331834216	-19.701	13.36916578	231.2281409
30	8.13320006	26.52751728	-6.331834216	-20.271	13.93916578	232.7339828
60	8.158078803	26.60866262	-12.66366843	-20.797	8.133331568	227.5974226
70	8.173018183	26.6573894	-14.77427984	-21.307	6.532720162	226.3987021
70	8.178	26.67363826	-14.77427984	-21.79	7.015720162	227.0157202

Errors					
X positive error	X negative erro	Ver fov up	Ver fov down	Y positive error	Y negative error
0.085638251	0.085638251	2.303792506	2.303792506	4.414403911	4.414403911
0.085601731	0.085570433	2.302810081	2.301968114	4.413421486	4.412579519
0.085460919	0.085398361	2.299022037	2.297339129	4.409633442	4.407950534
0.085215986	0.085122244	2.292432989	2.28991119	4.403044394	4.400522595
0.084867231	0.084742419	2.283050964	2.279693346	4.39366237	4.390304752
0.084415078	0.084259348	2.270887394	2.266698048	4.381498799	4.377309453
0.083860078	0.083673621	2.255957096	2.250941127	4.366568502	4.361552533
0.083202907	0.082985949	2.238278263	2.232441782	4.348889669	4.343053187
0.082444367	0.082197173	2.217872433	2.211222549	4.328483838	4.321833955
0.081585381	0.081308251	2.194764466	2.187309283	4.305375872	4.297920689
0.080626996	0.080320269	2.168982517	2.160731117	4.279593923	4.271342523
0.079570379	0.079234428	2.140557997	2.131520434	4.251169403	4.242131839
0.078416817	0.078052052	2.109525537	2.099712821	4.220136942	4.210324226
0.077167717	0.076774582	2.075922945	2.065347031	4.18653435	4.175958436
0.075824601	0.075403574	2.03979116	2.028464934	4.150402566	4.139076339
0.074389103	0.073940698	2.001174205	1.989111465	4.11178561	4.09972287
0.072862974	0.072387737	1.960119126	1.94733457	4.070730532	4.057945976
0.071248072	0.070746582	1.916675945	1.903185148	4.02728735	4.013796554
0.069546366	0.069019234	1.870897589	1.856716988	3.981508994	3.967328394
0.067759928	0.067207797	1.822839833	1.807986704	3.933451238	3.91859811
0.065890935	0.065314477	1.772561227	1.757053667	3.883172632	3.867665073
0.063941664	0.063341581	1.720123028	1.703979931	3.830734433	3.814591337
0.06191449	0.061291514	1.665589124	1.648830158	3.776200529	3.759441563
0.059811883	0.059166772	1.609025956	1.591671539	3.719637362	3.702282945
0.057636404	0.056969945	1.550502439	1.532573714	3.661113844	3.643185119
0.055390704	0.054703708	1.490089873	1.471608683	3.600701278	3.582220089
0.05307752	0.052370824	1.427861861	1.408850724	3.538473267	3.51946213
0.050699668	0.049974133	1.36389422	1.344376298	3.474505626	3.454987703
0.048260046	0.047516557	1.298264885	1.278263956	3.40887629	3.388875361
0.045761628	0.04500109	1.231053813	1.210594246	3.341665218	3.321205652
0.043207455	0.042430795	1.162342892	1.141449614	3.272954297	3.252061019
0.040600641	0.039808805	1.092215835	1.070914301	3.20282724	3.181525706
0.037944362	0.037138314	1.020758081	0.999074244	3.131369487	3.10968565
0.035241853	0.034422576	0.948056691	0.926016969	3.058668096	3.036628375
0.032496407	0.031664899	0.87420024	0.851831485	2.984811645	2.96244289
0.02971137	0.028868644	0.79927871	0.776608176	2.909890116	2.887219581
0.026890133	0.026037216	0.723383383	0.700438689	2.833994788	2.811050094
0.024036135	0.023174066	0.646606724	0.623415825	2.75721813	2.73402723
0.021152853	0.020282683	0.569042275	0.545633425	2.67965368	2.656244831
0.0182438	0.017366587	0.490784535	0.467186255	2.60139594	2.577797661
0.015312519	0.014429333	0.41192885	0.388169891	2.522540255	2.498781296
0.012362582	0.0114745	0.332571293	0.308680601	2.443182698	2.419292007
0.009397583	0.008505686	0.252808549	0.228815232	2.363419954	2.339426637
0.006421135	0.00552651	0.172737797	0.148671086	2.283349202	2.259282491
0.003436864	0.0025406	0.09245659	0.068345808	2.203067996	2.178957213
0.000448405	0	0.01206274	0	2.122674145	2.110611405

References				
λ_0 21cm line /m	c / vacuum / m/s	f 21cm line/ Hz	pi for conversion	solar orbit r / pc
0.211061141	299792458	1420405752	3.141592654	8178
LSR velocity km/s	1 AU in m	1 pc to m	1 ly to m	G constant
220	1.49598E+11	3.0857E+16	9.46053E+15	6.67428E-11
Solar mass				
1.988E+30				

Figure 26 - Microsoft Excel Spreadsheet used to organise data collection

Green columns represent input (values that were added onto the spreadsheet following data collection or from an external source), and red columns represent output data that was calculated using the input values. The unit and constant references, which were included in the Research Review, are shown in blue. The two columns shown in bold constitute the X and Y axes for the rotation curve.

Every formula and calculation used throughout this investigation is built into the spreadsheet, allowing for fast and efficient processing of raw data. An example of Excel syntax used is shown below:

L13 =K13+U$6*SIN(A13*(X$3/180))

This formula is used to calculate the Orbital velocity V of the signal source at l=20°, based on $V = V_{rec} + V_{\odot} \times sin(l)$.

L13 represents the cell in which V will be displayed.

K13 represents the corrected recessional velocity V_{rec}

A13 represents the galactic longitude at this point, l=20°

U$6 represents the reference for the LSR velocity of 220 km/s.

X$3 represents the reference for pi, which is used to convert longitude to radians, as Excel does not support degrees.

The constant references in this formula include the symbol $, which allows the spreadsheet to reference a single cell regardless of which row the formula is calculated for. For example, the formula for cell L36 will take values from K36 and A36, on the same row, but will still refer to cells U6 and X3.

6.2 Table of Results

Galactic longitude l / °	Orbital radius R / kpc	Minimum doppler frequency shift Δf_{min} / KHz	Topocentric recessional velocity V_{obs} / kms^{-1}	Local Standard of Rest correction V_{LSRK} / kms^{-1}	Corrected recessional velocity V_{rec} / kms^{-1}	Orbital velocity V / kms^{-1}
0	0	-150	31.7	13.128	18.53	18.53
2	0.2854	-160	33.8	12.341	21.43	29.11
4	0.5705	-180	38.0	11.539	26.45	41.80
6	0.8555	-190	40.1	10.724	29.38	52.37
8	1.138	-200	42.2	9.895	32.32	62.94
10	1.420	-240	50.7	9.053	41.60	79.80
12	1.700	-250	52.8	8.201	44.56	90.30
14	1.978	-290	61.2	7.339	53.87	107.1
16	2.254	-310	65.4	6.468	58.96	119.6
18	2.527	-340	71.8	6.851	64.91	132.9
20	2.797	-420	88.6	5.979	82.67	157.9
22	3.064	-540	114	5.101	108.9	191.3
24	3.326	-530	112	4.216	107.6	197.1
26	3.585	-520	110	3.325	106.4	202.9
28	3.839	-490	103	2.431	101	204.3
30	4.089	-510	108	1.534	106.1	216.1
32	4.334	-470	99.2	0.635	98.56	215.1
34	4.573	-440	92.9	-0.265	93.13	216.2
36	4.807	-370	78.1	-2.443	80.54	209.8
38	5.035	-370	78.1	-3.341	81.43	216.9
40	5.257	-350	73.9	-4.236	78.11	219.5
42	5.472	-320	67.5	-5.124	72.66	219.9
44	5.681	-300	63.3	-6.007	69.33	222.2

46	5.883	-290	61.2	-6.883	68.09	226.3
48	6.077	-280	59.1	-7.750	66.85	230.3
50	6.265	-270	57.0	-8.607	65.59	234.1
52	6.444	-240	50.7	-9.454	60.11	233.5
54	6.616	-210	44.3	-10.29	54.61	232.6
56	6.780	-160	33.8	-11.113	44.88	227.3
58	6.935	-140	29.5	-11.923	41.47	228.0
60	7.082	-130	27.4	-12.718	40.16	230.7
62	7.221	-100	21.1	-12.811	33.92	228.2
64	7.350	-80	16.9	-13.585	30.47	228.2
66	7.471	-40	8.44	-14.343	22.79	223.8
68	7.583	10	-2.11	-15.083	12.97	217.0
70	7.685	-10	2.11	-15.805	17.92	224.6
72	7.778	10	-2.11	-16.507	14.4	223.6
74	7.861	30	-6.33	-17.189	10.86	222.3
76	7.935	20	-4.22	-17.851	13.63	227.1
78	7.999	30	-6.33	-18.490	12.16	227.4
80	8.054	30	-6.33	-19.107	12.78	229.4
82	8.098	30	-6.33	-19.701	13.37	231.2
84	8.133	30	-6.33	-20.271	13.94	232.7
86	8.158	60	-12.7	-20.797	8.133	227.6
88	8.173	70	-14.8	-21.307	6.533	226.4
90	8.178	70	-14.8	-21.790	7.016	227.0

6.3 Specification of Significant Figures

Throughout the spreadsheet calculations, no values were rounded until the final answer, and instead the exact numerical values for each quantity were used. This is to maintain accuracy throughout all calculations and avoid unnecessary rounding errors.

However, the table of results requires a consistent number of significant figures for each column, based on the precision to which each value is known. Including an unnecessarily large number of significant figures unbacked by scientific precision would be impractical and clutter the table.

Each calculated result on the spreadsheet was rounded to an appropriate number of significant figures using the =ROUND() function.

V_{rec}, V and R are rounded to four significant figures each
V_{obs} is rounded to three significant figures.
The unaltered quantities of Δf and V_{LSRK} were kept at their original number of significant figures, as both quantities originate from primary sources (data collection and a NRAO calculator).

Furthermore, the rotation curve will be plotted using the unrounded values, and instead error bars will be used to indicate measurement uncertainties.

6.4 Uncertainties and Error Bars

The uncertainties in this experiment are primarily due to the resolution of the 12-metre radio telescope. With the chosen data collection settings, the telescope has a frequency resolution of 10 KHz, which contributes a maximum uncertainty of ± 2.11 km/s on the Y-axis, as a result of using the Doppler formula.

Moreover, with chosen data collection settings, the telescope has a half-power beam width of 1.2°. This means that the signal source's longitude has an uncertainty of ± 0.6°, and thus all calculations involving sin(l) will be affected. This results in a small but noteworthy error for both the X and Y-axes. Because sin(l) does not have a constant gradient, the upper and lower error bounds will be different and must be individually computed.

The above errors were organised in the Excel Spreadsheet and included in the rotation curve (Figure 27) as error bars.

Additional random errors may be caused by changes in galactic latitude b°, and the observed point appearing to drift out of view" as the Earth rotates. However, these errors are less significant, and their calculation would be unnecessarily complex given the experimental method used, as all observed points were at b=0 and thus latitude was not included as a parameter in any calculations.

6.5 Plotting the Rotation Curve

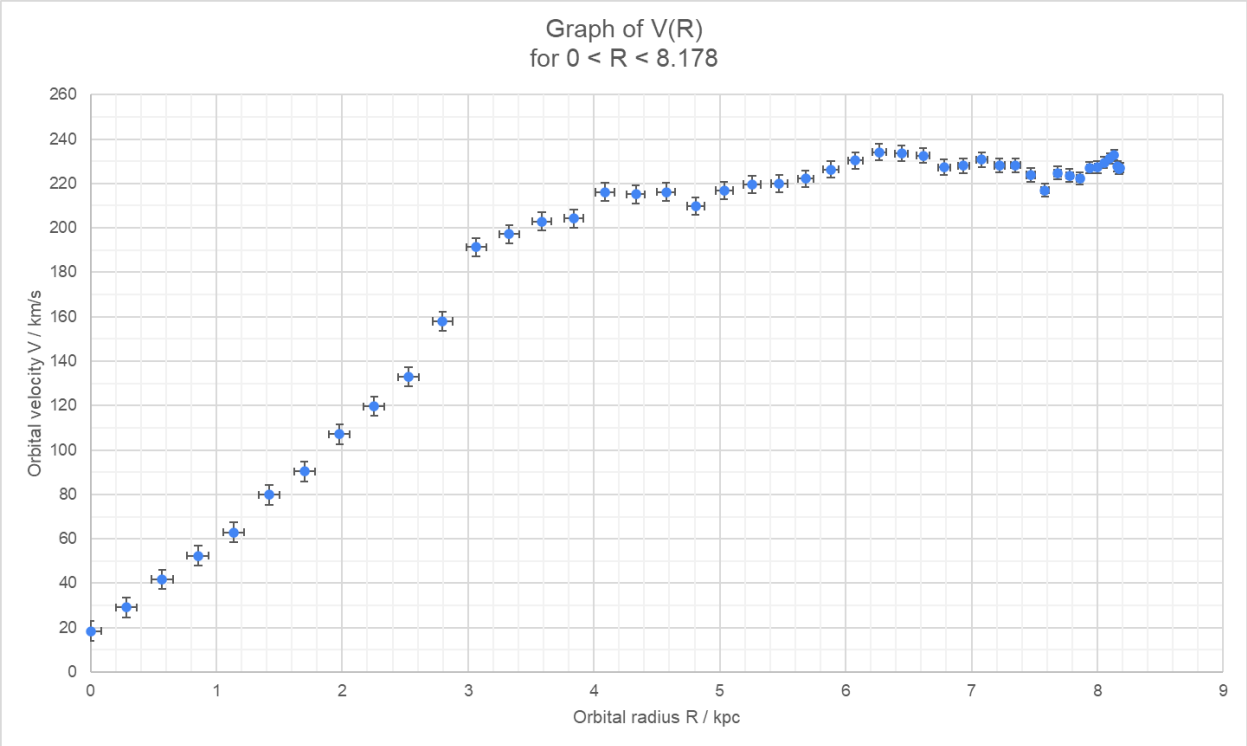

Figure 27 (Final Result) - Graph of V(R) for 0 < R < 8.178

The graph of Orbital velocity V against Orbital radius R is plotted in Microsoft Excel. The above-stated errors are plotted as error bars.

7. Interpretation

7.1 Mass Distribution and Comparison to Keplerian Hypothesis.

The rotation curve of V(R), shown in Figure 27, is concordant with the literature and cited papers in the Research Review. My result for V(R) shows orbital velocity flattening out after approximately 4 kpc, to a consistent range between 200 - 240 km/s.

This feature is strongly inconsistent with a Keplerian model where most of the Galaxy's visible mass is located within a central bulge, interior to the Sun's orbit. According to Kepler's Third Law, and Newton's Law of Gravitation, orbital velocity V would be expected to exponentially decay by a factor of $\frac{1}{\sqrt{R}}$, as long as the interior mass is constant.

The flattened rotation curve determined in this paper suggests that the concentration of matter in our Galaxy extends further beyond the Sun's orbit, as unusually high orbital velocities are sustained at large radii.

To further analyse the mass distribution, the orbital velocity equation from 3.6 was re-derived to make enclosed mass M the subject:

$$V = \sqrt{\frac{GM}{R}}$$

$$V^2 R = GM$$

$$M = \frac{V^2 R}{G}$$

The enclosed mass was calculated and plotted against the orbital radius in Figure 28. The gradient of the graph represents the mass concentration at a certain point, and it shows no consistent decrease towards larger radii as expected from photometric data.

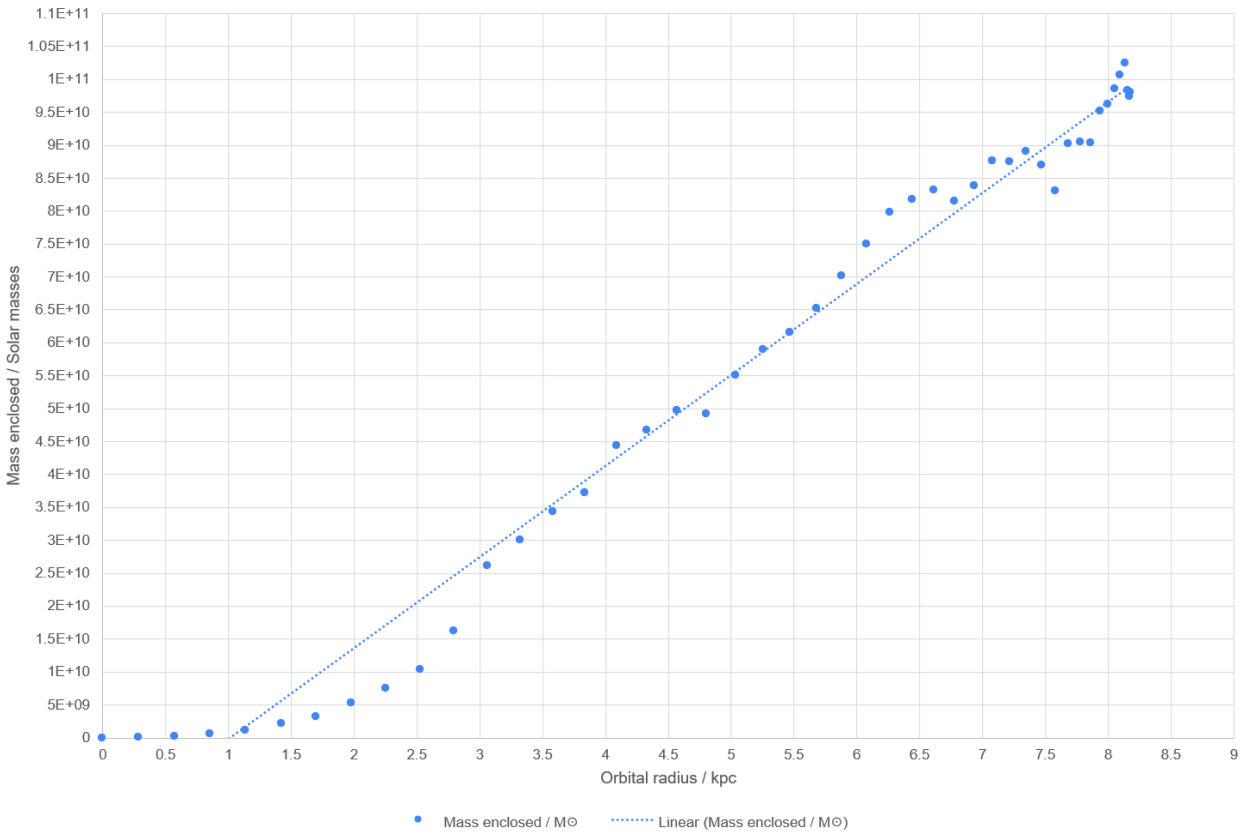

Figure 28 - Mass distribution in the Milky Way up to 8.18kpc

For galactocentric distances under 3kpc, data is affected by systematic error, and shows an incorrect distribution. This systematic error will be covered in detail in the Discussion. However, at radii above 3kpc, the mass distribution graph is consistent with the literature, showing a linear relationship and no sign of decrease, suggesting that matter density is constant towards the Sun's orbit and beyond.

7.2 Nature of Relative Intensity Peaks

The interpretation of raw data samples from this investigation can provide additional insight into galactic structure, as well as the accuracy and reliability of the data collected.

A notable feature observed across several individual spectrum graphs, particularly at higher longitudes where background noise is less obtrusive, was the emergence of multiple strong intensity peaks. Rather than a uniform peak within the spectrum, these irregularities begin to reveal the intriguing complexity of galactic structure.

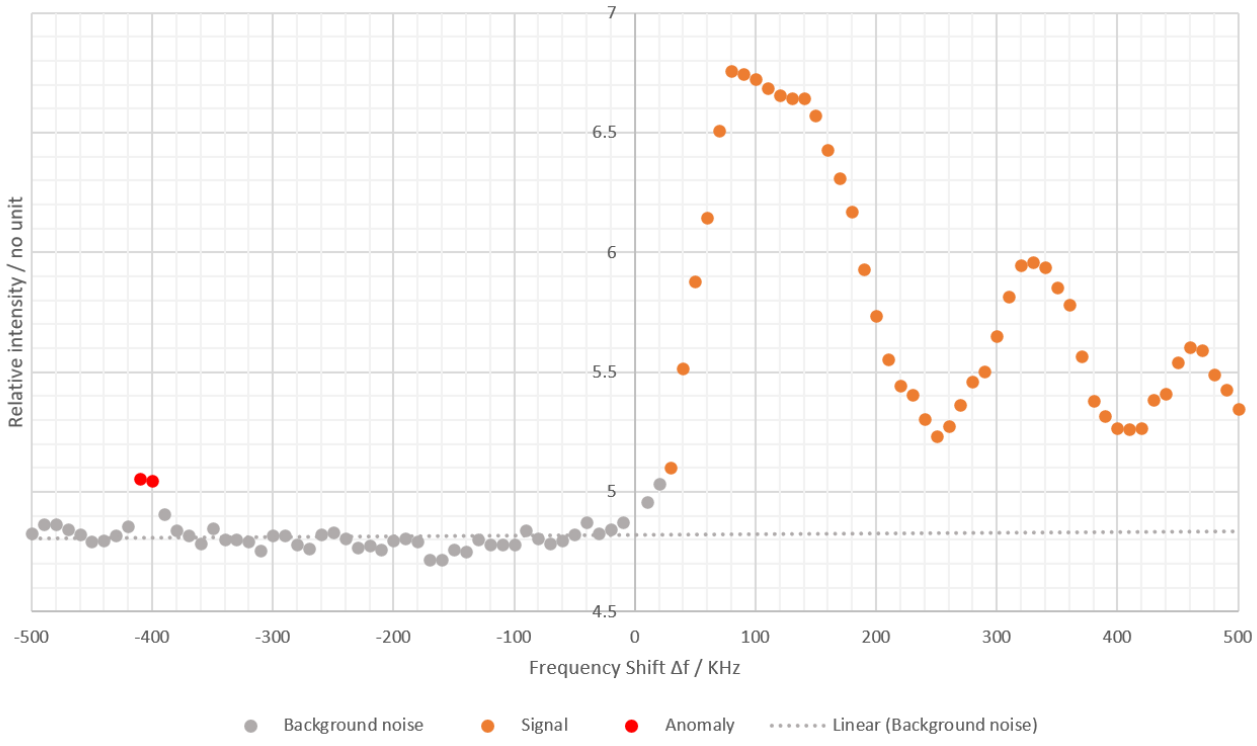

Figure 29 - Spectrum graph at l=82° showing multiple distinct intensity peaks

An analysis of Figure 29 the existence of three peaks in the spectrum. In this case, the peaks are widely separated, and therefore the sources emitting them are moving at appreciably different velocities, suggesting there may be several spiral arms of the Milky Way within the direction of observation. This is

an important distinction, as only the most red-shifted signal can be used for the tangent-point method, corresponding to the source with the lowest orbital radius.

At other points, the spectrum graph shows multiple, which are less spread out from one another compared to the previous example. Figure 30 shows the spectrum graph of l=90°, including less distinct intensity peaks.

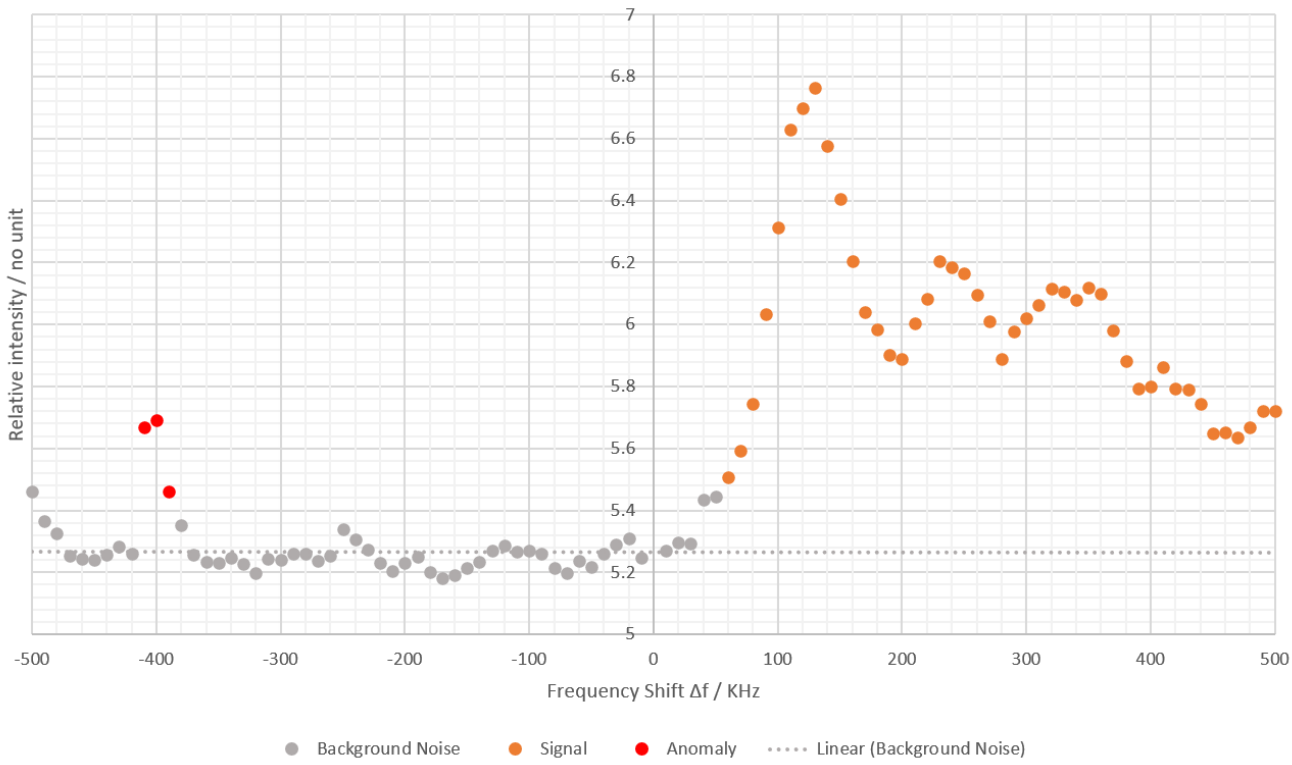

Figure 30 - Spectrum graph at l=90° showing a more compact signal with less prominent individual peaks

The above spectrum is likely to originate from a single larger source, such as a gas cloud with small differences in velocity throughout its vast structure. A rotating or expanding feature would explain this phenomenon. In either case, the entire structure is moving relative to us, while one side is receding and the other is moving towards us.

7.3 Local Velocity Dispersion

Radio signal sources such as cold hydrogen gas clouds are anisotropic. This means that velocity distribution is not uniform throughout the signal source, and distinct parts of the gas cloud are moving at different velocities, leading us to receive a range of Doppler-shifted frequencies rather than a single exact frequency shift.

The width (frequency range) of a signal can allow us to determine the magnitude of random local motions within the signal source. Liu & Chronopoulos proposed in 2008 that the signals observed in the line of sight at l=180° would not have a net Doppler shift, and therefore the signal width at this longitude is only indicative of local velocity dispersions. As shown in Figure 31, this point was scanned and a signal width of 160 KHz was obtained, corresponding to a velocity dispersion value of 34 km/s, which is larger than the previously mentioned paper.

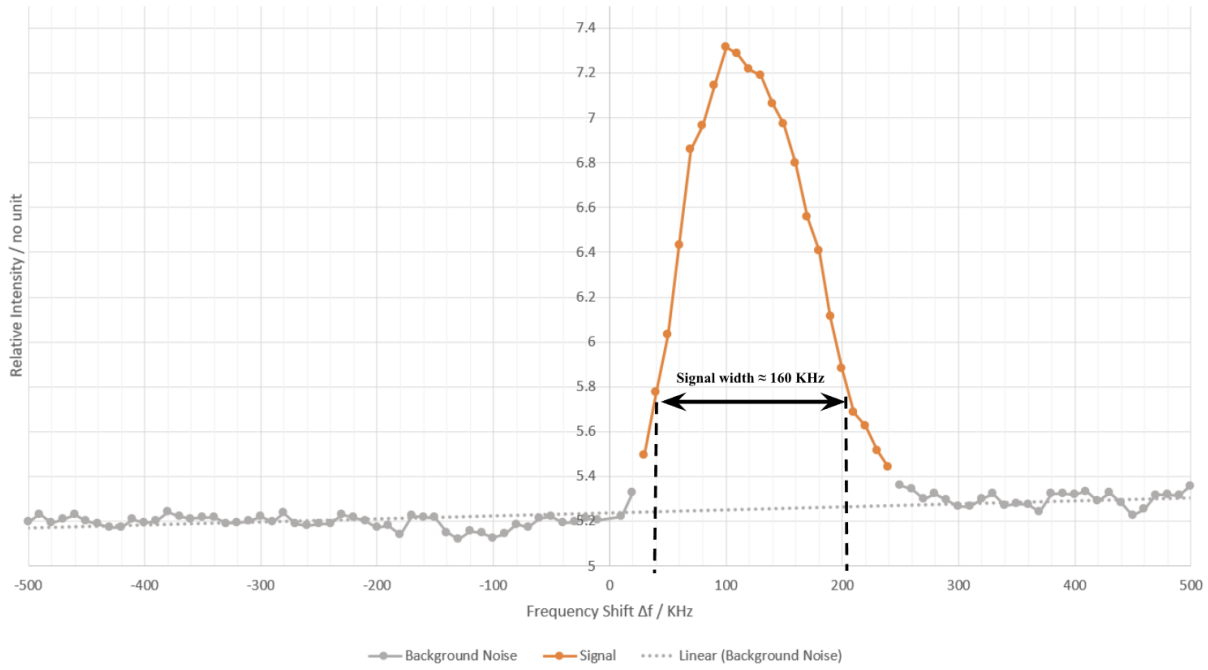

Figure 31 - Spectrum graph at l=180° showing a more compact signal with less prominent individual peaks

In contrast to the results obtained by Liu & Chronopoulos, my spectrum graph shows an overall blueshift, corresponding to a signal source moving towards us. This is because of the different frames of reference used, as my result for this section is not adjusted to a heliocentric standpoint.

7.4 Fluctuations in the Background Noise

The background noise level in a spectrum graph represents the overall intensity of unwanted radio emissions from varying sources. Radio noise can originate from inside the antenna's receiver, in the form of "thermal noise," from the functioning of electrical components and caused by the vibration of atoms in a component. (Hum, S.V.) Radio noise can also originate from external sources, such as the uniform emission of radio frequencies near the Galactic Centre, and in the Earth's atmosphere, caused by electrical discharges and other phenomena. The intensity of background noise from an observed region in the sky can provide an indication of the average concentration of radio-emitting matter in that region, from which we can infer the matter density in that region.

In the absence of calibration, the level of background noise is measured by the unitless quantity of relative intensity (as mentioned in the Instrumentation section). These uncalibrated values, however, can be compared to one another, as the telescope gain was kept constant throughout all observations. Figures 32 and 33 show a plot of background noise intensity for multiple values of l. Across the observation range, the relative intensity of background noise is observed to decrease as longitude increases from 0° to 90°. (**Figure 34**).

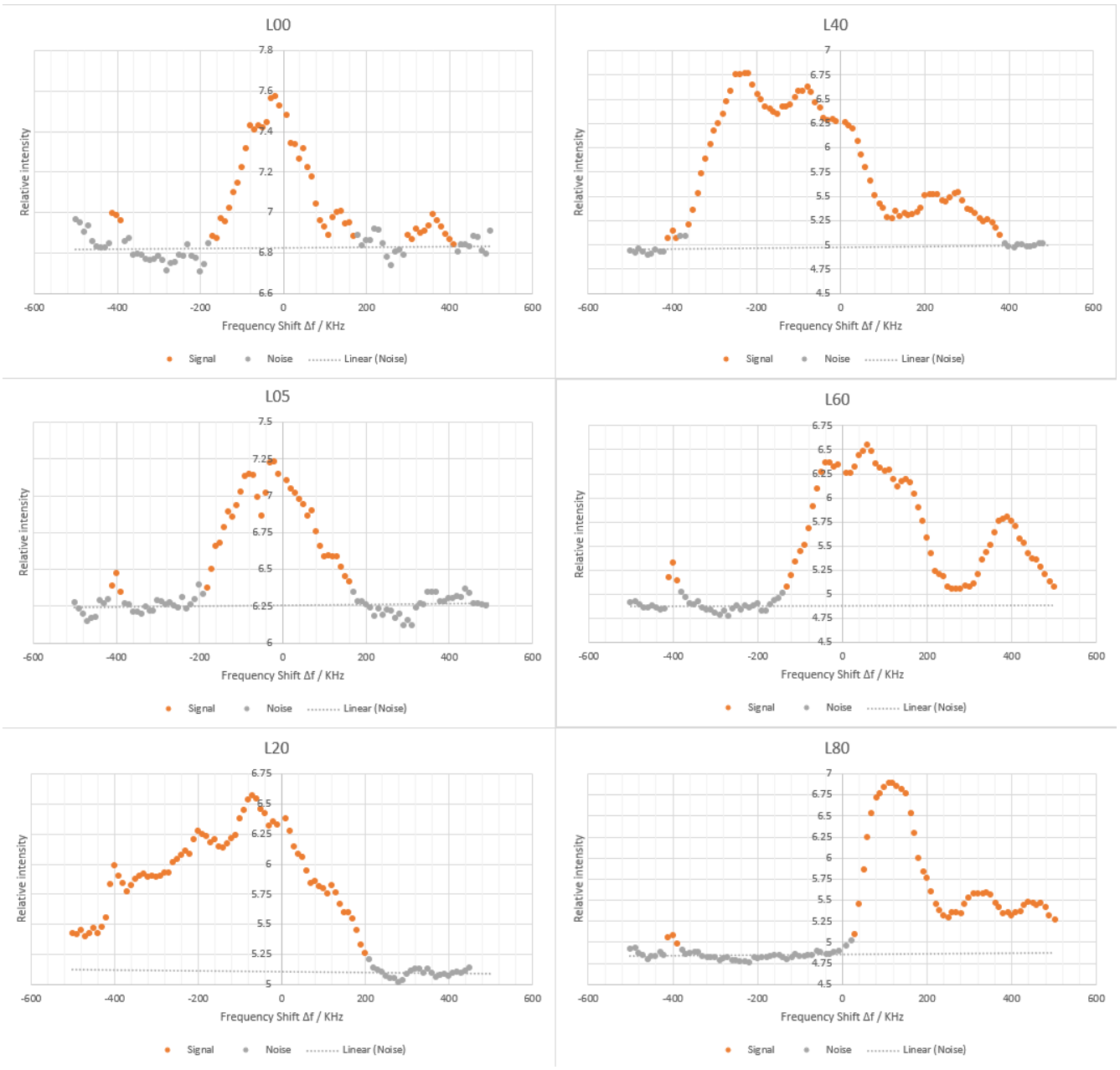

Figure 32 - Spectrum graphs showing noise (in grey) and H I signal intensities (orange) for l=0,5,20,40,60,80

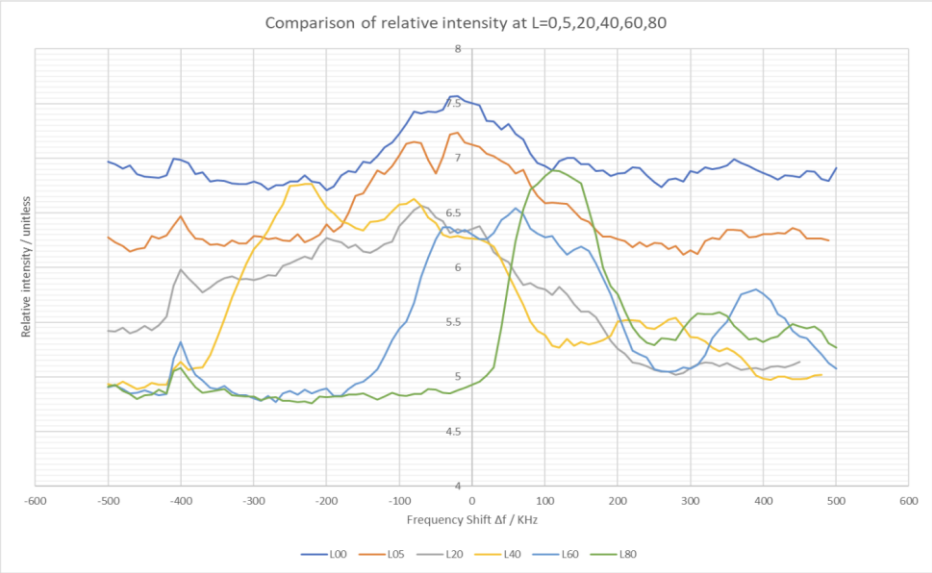

Figure 33 - Comparison of spectrum graphs for l=0,5,20,40,60,80

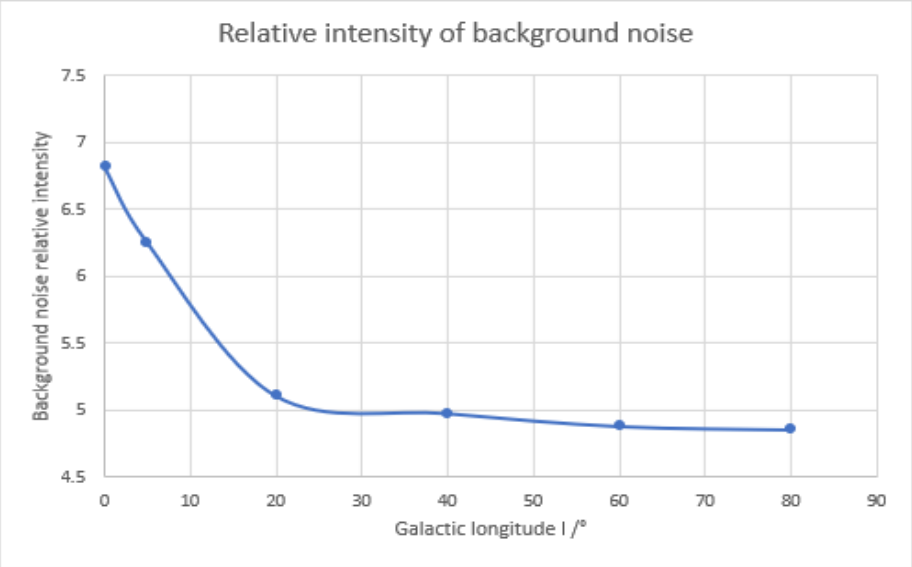

Figure 34 - Graph of background noise against galactic longitude l (right)

The large amount of noise in the vicinity of the Galactic Centre is owed partly to its position in the sky. At the time of observation, points with small longitudes were very close to the horizon, such that H I signal from the Galaxy must travel a longer distance through the atmosphere, resulting in increased noise.

7.5 Anomalies

Throughout the data collection process, a small intensity peak was identified within the frequency range $-410 < \Delta f < -390$ KHz ($f \approx 1420.005$ MHz). This peak is consistent throughout nearly all data samples, across several observation sessions. Although it appears to be above the significant noise threshold (an increase of more than 5% from the noise background), it is classified as an anomaly and ignored when determining Δf_{min}. Figure 35 shows instances of this peak in several observations:

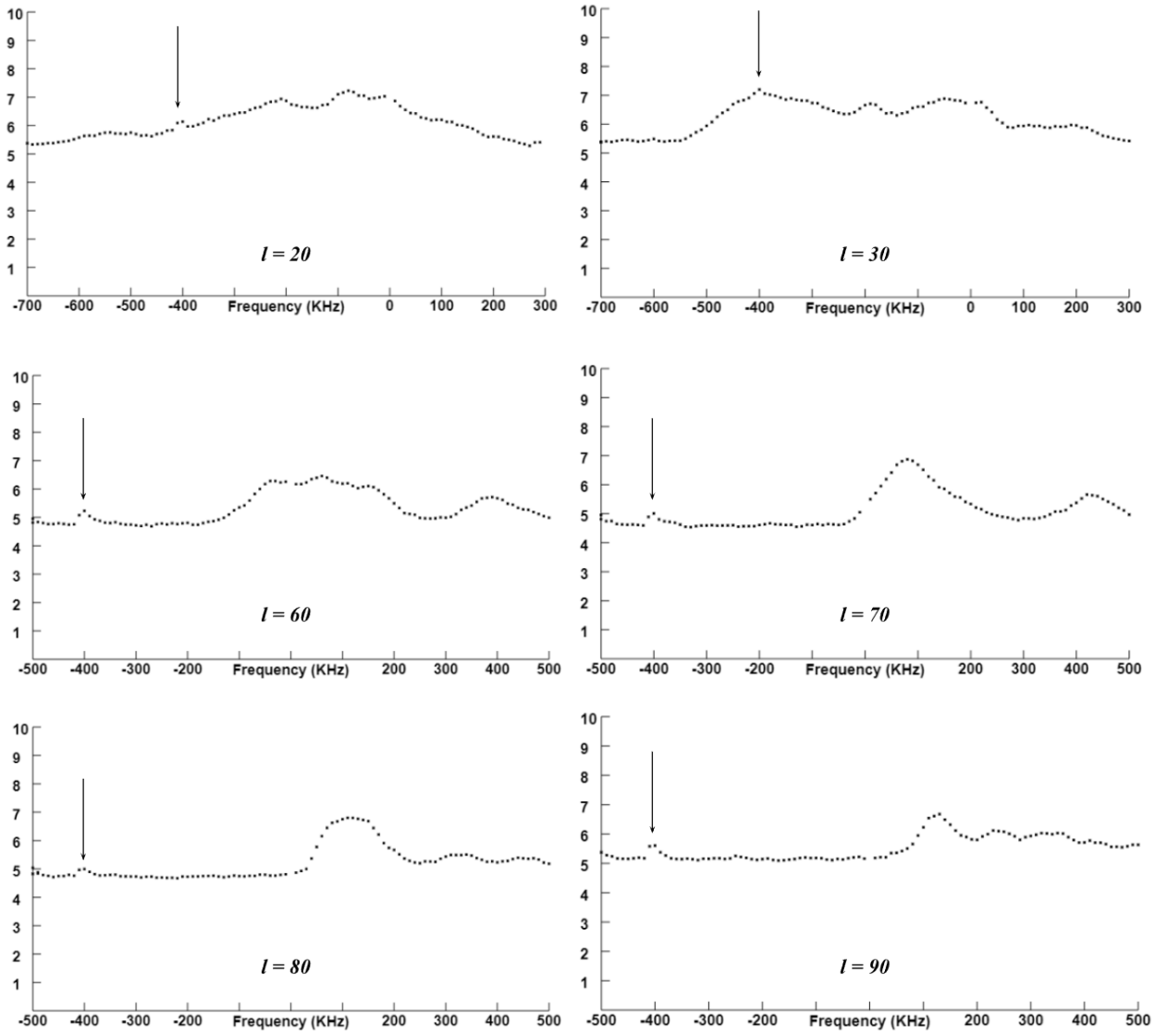

Figure 35 - The Anomaly is shown to be consistent at various galactic longitudes.

The Anomaly has also been identified in the past at PARI, although its source has not been confirmed. Several other perturbations in the spectrum were occasionally identified. However, they were temporary and likely caused by a passing object (a bird, or perhaps a satellite) interfering with telescope readings. When detected, the scan was repeated until there were no signs of visible interference.

8. Discussion

Throughout this investigation, there were a few sources of systematic error that are very difficult to determine quantitatively. While they do not have a negative impact on the reliability of these results, it is still important to describe them.

8.1 Systematic error - The Galactic Bar

The tangent-point method is rooted in the assumption that orbits within the galaxy are circular. In the case of non-circular orbits, galactic geometry becomes far more complex. This assumption is accurate for the outer regions of the galaxy, including the region in which our Sun orbits. However, in the proximity of the Galactic Centre, there is a region known as the Galactic Bar. This structure contains densely concentrated luminous matter, including stars and hot gas clouds, containing somewhat irregular and non-circular orbits. The galactic bar has been estimated to extend 2.5kpc in length (Babusiaux & Gilmore, 2005) and 3.5kpc (Bissantz & Gerhard, 2002), from the Galactic Centre, angled at approximately 22° from the Sun-Galactic Centre line of sight (Babusiaux & Gilmore, 2005).

Furthermore, orbits within the Galactic Bar also extend outside the plane of the galactic disk, making the tangent-point model inaccurate for observations in the bar area, as velocity and radius calculations are incorrect.

It was found by Chemin et al. in 2015 that recessional velocities for radii up to 4 kiloparsecs could be affected by considerable velocity dispersion in the vicinity of the source. However, the study found that the results obtained by the tangent-point method are very accurate and consistent with other methods within the range $4.5 < R \leq 8$ kpc, where a flat rotation curve is observed. This supports the reliability of my interpretation that V(R) is inconsistent with a Keplerian model, in the absence of "invisible dark matter."

8.2 Systematic error - Extremum Longitudes

Another notable limitation of the tangent-point method is that, as the line of sight approaches the Local Standard of Rest velocity vector (l=90°), and the Galactic Centre (l=0), signals will have a very small relative velocity compared to the dispersion of random local velocities, causing Δf_{min} to be less representative of rotational velocity.

Furthermore, the ≈ 2.1km/s uncertainty caused by the telescope's frequency measurement resolution becomes more significant when compared to small relative velocities at these longitudes. While this error may account for up to 32% of the corrected recessional velocity at l=88°, and 12% at l=0°, it is inconsequential at most longitudes.

8.3 Systematic error - Galactic Constants

The most fundamental source of error in this investigation stems from the uncertainty surrounding the Galactic Constants. As previously mentioned, estimates for $V_\odot$ range from 200 km/s, or even 180 km/s in earlier studies, up to as high as 250 km/s. The Galactocentric Distance $R_\odot$ is better known, but recent estimates still range from anywhere between 8 - 8.5kpc. This is, in part, due to the considerable differences between methods in these studies.

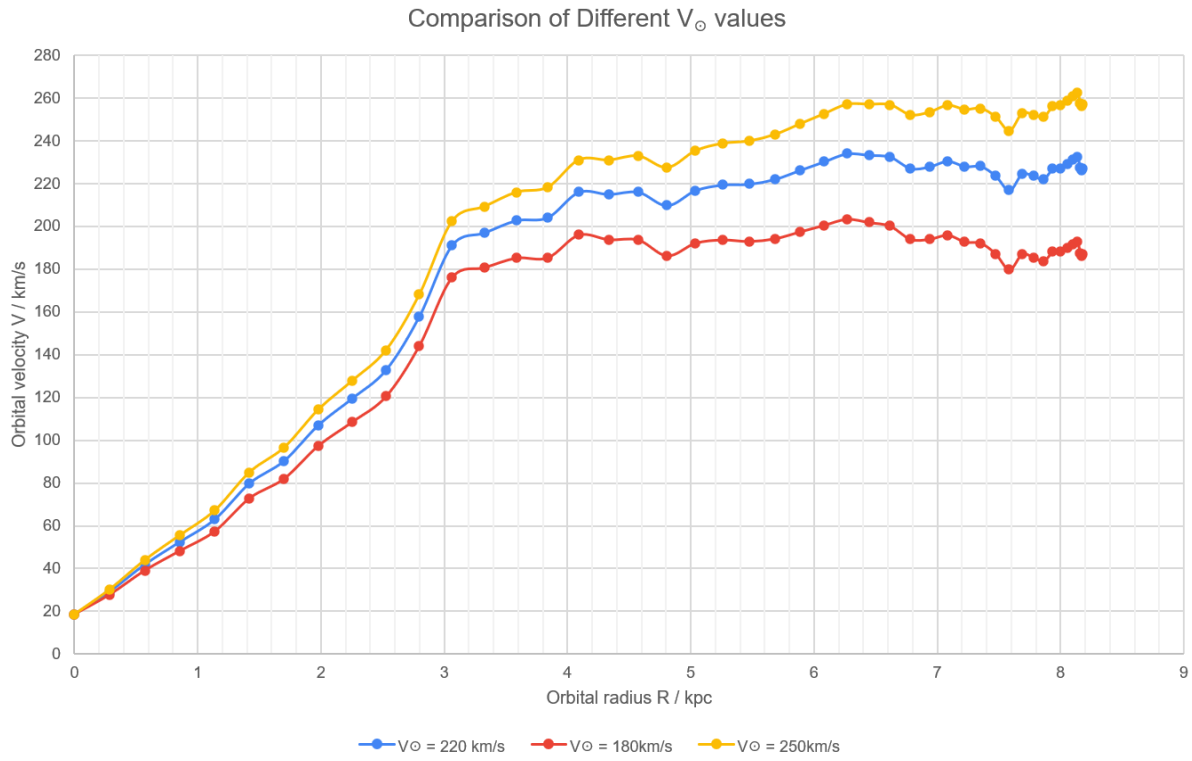

Figure 36 - Comparison of the V(R) curve determined in this investigation, using different values for $V_\odot$

While different values for $R_\odot$ merely scale the graph differently on the x-axis, changes in $V_\odot$ have a sizeable impact on the shape of the rotation curve, leading to vastly different interpretations of galactic mass distribution. To determine an accurate rotation profile for the Milky Way Galaxy, the Galactic Constants $V_\odot$ and $R_\odot$ must be confidently established.

9. Conclusion

The Milky Way has fascinated humanity, arguably ever since the first human looked up at the night sky. However, it took thousands of years for us to understand that the dusty band is actually a complex system of stars, gas and dust.

Earth's position within the galaxy has not been advantageous to galactic research, as dense clouds of dust pervade the interstellar medium and obstruct light from the galactic centre. Visible light wavelengths are most affected, but longer wavelengths such as infrared or radio are hardly affected at all. Thus, the field of radio astronomy revolutionised galactic research entirely, allowing an unprecedented perspective of the Milky Way.

In this paper, the depths of radio astronomy, spectroscopy and orbital mechanics as fields of research were analysed in great detail, encapsulating the scientific context of the Milky Way's dynamics and laying the foundation for investigating the rotation curve of the galaxy. I took Doppler shift measurements in the spectrum of neutral hydrogen at a wavelength of 21 cm, using the 12-metre radio telescope at the Pisgah Astronomical Research Institute. A well-established "tangent-point" method was used to determine the distance to observed radio sources, by measuring the most red-shifted signal and trigonometrically computing its distance and velocity with respect to the Galactic Centre.

According to Keplerian orbital mechanics, and the expected mass distribution from visible light observations, the galaxy's rotation should slow towards its outer regions, with orbital velocity decreasing proportionally with $1/\sqrt{r}$. However, following extensive observation, a flat rotation profile was determined from 3.5 kpc. The results were conclusive and in stark contrast to the hypothesis, indicating that the galaxy's mass density remains relatively constant towards the Sun's orbit and beyond. One well-founded explanation is the existence of "dark matter," representing invisible matter which only interacts gravitationally, and is thus impossible to detect directly. Although it has been proposed in academic research since the 1970s, its actual nature remains unknown to this day.

The outcome of this investigation is in agreement with prominent literature such as the research of Sofue (2020) and Liu & Chronopoulos (2008), with many applications to our understanding of the galaxy, confirming and reinforcing the existence of dark matter. Additional research could be done using this data to determine a mathematical model for dark matter around the galaxy and to calculate its total mass. Furthermore, a similar method could be employed to investigate and determine the spiral structure of the

Milky Way and the shape of orbits inside it. Moreover, as the Galactic Constant values contributed the greatest uncertainty to this investigation, perhaps the greatest improvement to its accuracy could be made by narrowing down the Sun's orbital radius and velocity to precise values.

Ultimately, the results obtained in this paper strengthen the past century's galactic research, while providing a new perspective through the usage of PARI's 12-metre radio telescope, and an increased amount of observation data points, prompting further efforts to elucidate the enigmatic dark matter.

10. Works cited

10.1 Figure Links

Figure 1 - The emission of a visible spectral line from a hydrogen atom.
Credit: JabberWok, 2007 CC BY-SA 3.0 <http://creativecommons.org/licenses/by-sa/3.0/> , via Wikimedia Commons

Figure 2 - The spin-flip transition
Credit: © Swinburne University of Technology. Retrieved from https://astronomy.swin.edu.au/cosmos/s/Spin-flip+Transition

Figure 3 - The basic structure of a radio telescope antenna
Credit: © 2023 The National Radio Astronomy Observatory. Retrieved from https://public.nrao.edu/telescopes/radio-telescopes/

Figure 4 - The Relativistic Doppler effect for light
Credit: Relativistic Doppler Shift - HyperPhysics (©C.R. Nave, 2017) - Georgia State University

Figure 5 - Conventions for the non-relativistic Doppler effect: Optical (left), Radio (right)

Credit: National Radio Astronomy Observatory - Guide to Observing with the VLA - Spectral Line

Figure 6 - The radial components of Earth and the Source's velocities.

Own work, created as a Google Docs Drawing.

Figure 7 - The apparent relative motion of local stars due to the Sun's peculiar motion.

Credit: Solar Motion. Case Western Reserve University (2023). Notes for the course Str222. Retrieved from http://burro.case.edu/Academics/Astr222/Galaxy/Kinematics/solarmotion.html

Figure 8 - Graph of the orbital velocity of Solar system planets (and Pluto).

Credit: Chris Palma. The Rotation Curve of the Milky Way. ASTRO 801 Lesson 8 - The Milky Way Galaxy. Penn State University. Retrieved from https://www.e-education.psu.edu/astro801/content/l8_p8.html

Figure 9 - The averaged rotational curve of the Milky Way galaxy in the 0-50 kpc range

Credit: Sofue, Yoshiaki (2020). *Rotation Curve of the Milky Way and the Dark Matter Density*. Retrieved from: https://arxiv.org/pdf/2004.11688.pdf

Figure 10 - The dark matter halo and its effects on the rotation curve.

Credit: Nick Strobel (2022). Bakersfield College. AstronomyNotes.com. Retrieved from https://www.astronomynotes.com/ismnotes/s7.htm

Figure 11 - Stellar parallax and the definition of a Parsec

Credit: Astronomy Stack Exchange, 2013. Original file from Cosmic Reference Guide (Caltech) no longer available online

Retrieved from: https://astronomy.stackexchange.com/questions/94/what-is-a-parsec-and-how-is-it-measured

Figure 12 - Two angles of the 12-metre radio telescope, on July 17th, 2023.

Own photo, taken at the Pisgah Astronomical Research Institute.

Figure 13 - 12-metre telescope control interface

Credit: Pisgah Astronomical Research Institute, Retrieved from http://12m.pari.edu, login required

Figure 14 - The Horizontal Coordinate System

Credit: TWCarlson, CC BY-SA 3.0 <https://creativecommons.org/licenses/by-sa/3.0>, via Wikimedia Commons

Figure 15 - The Equatorial Celestial Sphere

Credit: © Swinburne University of Technology. Retrieved from

https://astronomy.swin.edu.au/cosmos/E/Equatorial+Coordinate+System

Figure 16 - Right Ascension, Declination and the Ecliptic

Credit: Tfr000 (yhhbhhiijnbyuygggtalk) 15:34, 15 June 2012 (UTC), CC BY-SA 3.0 <https://creativecommons.org/licenses/by-sa/3.0>, via Wikimedia Commons

Figure 17 - Galactic coordinates (longitude and latitude)

Credit: Brews ohare, CC BY-SA 3.0 <https://creativecommons.org/licenses/by-sa/3.0>, via Wikimedia Commons

Figure 18 - The spectral profile of H I observation in the line of sight, containing signal peaks from different gas clouds.

Credit: Carroll & Ostlie (2007). Introduction to Modern Astrophysics. p. 914, Fig. 24.24

Figure 19 - Conversion from Galactic to Equatorial coordinates

Credit: Carroll & Ostlie (2007). Introduction to Modern Astrophysics. p. 901, eq. 24.19, 24.20, 24.21

Figure 20 - The Coordinate Transformation calculator interface at https://ned.ipac.caltech.edu/forms/calculator.html

Credit: NASA/IPAC Extragalactic Database Coordinate Transformation & Galactic Extinction Calculator. Hosted by Caltech.

Figure 21 - Graphs of altitude over time for reference stars near galactic longitudes l = 0, 20, 40, 60

Own work, Exported from the Stellarium software (stellarium.org)

Figure 22 - Scan of l = 44° including noise background and line showing minimum significant intensity.

Own work, created as a Google Docs drawing

Figure 23 - Low-velocity Doppler shift expression (cropped from original source)

Credit: C.R. Nave (2017). HyperPhysics - Georgia State University

Figure 24 - Radial velocity calculator for the Green Bank Telescope.

Credit: National Radio Astronomy Observatory. Retrieved from: https://www.gb.nrao.edu/cgi-bin/radvelcalc.py

Figure 25 - Geometry used to calculate the orbital radius and velocity of the observed object

Own work, created as a Google Docs drawing

Figure 26 - Microsoft Excel Spreadsheet used to organise data collection

Own work, created in Microsoft Excel

Figure 27 - Graph of V(R) for 0 < R < 8.178, bas

Created in Microsoft Excel

Figure 28 - Mass distribution in the Milky Way up to 8.18kpc

Created in Microsoft Excel

Figure 29 - Spectrum graph at l=82° showing multiple distinct intensity peaks

Own work, created in Microsoft Excel

Figure 30 - Spectrum graph at l=90° showing a more compact signal with less prominent individual peaks

Own work, created in Microsoft Excel

Figure 31 - Spectrum graph at l=180° showing a more compact signal with less prominent individual peaks

Own work, created in Microsoft Excel

Figure 32 - Spectrum graphs showing noise (in grey) and H I signal intensities (orange) for l=0,5,20,40,60,80

Own work, created in Microsoft Excel

Figure 33 - Comparison of spectrum graphs for l=0,5,20,40,60,80

Own work, created in Microsoft Excel

Figure 34 - Graph of background noise against galactic longitude l

Own work, created in Microsoft Excel

Figure 35 - The Anomaly is shown to be consistent at various galactic longitudes.

Own work, created as a Google Docs drawing.

Figure 36 - Comparison of the V(R) curve determined in this investigation, using different values for $V_{\odot}$

Own work, created in Microsoft Excel

10.2 Reference List

Abuter, R., Amorim, A., Bauböck, M., Berger, J.P., Bonnet, H., Brandner, W., Clénet, Y., Coudé du Foresto, V., de Zeeuw, P.T., Dexter, J., Duvert, G., Eckart, A., Eisenhauer, F., Förster Schreiber, N.M., Garcia, P., Gao, F., Gendron, E., Genzel, R., Gerhard, O. and Gillessen, S. (2019). A Geometric Distance Measurement to the Galactic Center Black Hole with 0.3% Uncertainty. *Astronomy & Astrophysics*, 625(L10). doi:https://doi.org/10.1051/0004-6361/201935656.

Australia Telescope National Facility (2019). *How does a radio telescope work?* [online] Australia Telescope National Facility. Available at: https://www.atnf.csiro.au/outreach/education/pulseatparkes/radiotelescopeintro.htm [Accessed Aug. 2023].

Babusiaux, C. and Gilmore, G. (2005). The structure of the Galactic bar. *Monthly Notices of the Royal Astronomical Society*, [online] 358(4), pp.1309–1319. doi:https://doi.org/10.1111/j.1365-2966.2005.08828.x.

Bertone, G. and Hooper, D. (2018). History of Dark Matter. *Reviews of Modern Physics*, [online] 90(045002). doi:https://doi.org/10.1103/revmodphys.90.045002 .

Bissantz, N. and Gerhard, O. (2002). Spiral arms, Bar Shape and Bulge Microlensing in the Milky Way. *Monthly Notices of the Royal Astronomical Society*, [online] 330(3), pp.591–608. doi:https://doi.org/10.1046/j.1365-8711.2002.05116.x.

Blaauw, A., Gum, C.S., Pawsey, J.L. and Westerhout, G. (1960). The New I. A. U. System of Galactic Coordinates (1958 Revision). *Monthly Notices of the Royal Astronomical Society*, [online] 121(2), p.123. Available at: https://adsabs.harvard.edu/full/1960MNRAS.121..123B [Accessed Aug. 2023].

Blitz, L. and Spergel, D.N. (1991). Direct Evidence for a Bar at the Galactic Center. *Astrophysical Journal*, [online] 379, p.631. doi:https://doi.org/10.1086/170535.

Britannica, The Editors of Encyclopaedia (n.d.). *Angular Displacement | Physics | Britannica*. [online] Encyclopedia Britannica. Available at: https://www.britannica.com/science/angular-displacement [Accessed Aug. 2023].

Britannica, The Editors of Encyclopaedia (n.d.). *Experimental Study of Gravitation*. [online] Encyclopedia Britannica. Available at: https://www.britannica.com/science/gravity-physics/Experimental-study-of-gravitation#ref210893 [Accessed Aug. 2023].

Britannica, The Editors of Encyclopaedia (n.d.). *Meridian Definition & Meaning | Britannica Dictionary*. [online] Encyclopedia Britannica. Available at: https://www.britannica.com/dictionary/meridian [Accessed Aug. 2023].

Britannica, The Editors of Encyclopaedia (2023). *Vernal Equinox | Definition, Dates, & Facts*. [online] Encyclopedia Britannica. Available at: https://www.britannica.com/science/vernal-equinox .

Brown, R.L. (n.d.). *Historical Introduction to Radio Astronomy | Lecture 10*. [online] California Institute of Technology Department of Astronomy. Available at: https://sites.astro.caltech.edu/~srk/Ay126/Lectures/Lecture10/Brown_RadioAstronomy.pdf [Accessed Aug. 2023].

Burke-Spolaor, S. (n.d.). *ASTR469 Lectures 7–8: Coordinates (Ch. 1)*. [online] West Virginia University. Available at: https://sarahspolaor.faculty.wvu.edu/files/d/bff87be8-3998-4745-9a00-7d57560f261d/07_notes.pdf [Accessed Aug. 2023].

Burton, W.B. and Gordon, M.A. (1978). Carbon Monoxide in the Galaxy. III. the Overall Nature of Its Distribution in the Equatorial plane. *Astronomy and Astrophysics*, [online] 63(1-2), pp.7–27. Available at: https://articles.adsabs.harvard.edu/full/1978A%26A....63....7 B [Accessed Aug. 2023].

Cabrera-Lavers, A., Hammersley, P.L., González-Fernández, C., López-Corredoira, M., Garzón, F. and Mahoney, T.J. (2007). Tracing the Long Bar with Red-clump Giants. *Astronomy & Astrophysics*, 465(3), pp.825–838. doi:https://doi.org/10.1051/0004-6361:20066185.

Carroll, B.W. and Ostlie, D.A. (2007). *An Introduction to Modern Astrophysics*. Pearson International Edition ed. San Francisco: Pearson Addison-Wesley, pp.2–36, 202–209, 398–411, 881–922.

Chemin, L., Renaud, F. and Soubiran, C. (2015). Incorrect Rotation Curve of the Milky Way. *Astronomy & Astrophysics*, [online] 578, p.A14. doi:https://doi.org/10.1051/0004-6361/201526040.

Chiu, C.K. and Strigari, L.E. (2020). Testing the Accuracy of the Tangent Point Method for Determining the Milky Way's Inner Rotation Curve. *Research Notes of the AAS*, [online] 4(9), p.165. doi:https://doi.org/10.3847/2515-5172/abbad8.

Christensen, N.L. (n.d.). *Measurement of Galactic Rotation Curve* . [online] *Advanced Physics Laboratories*. University of Michigan. Available at: http://instructor.physics.lsa.umich.edu/adv-labs/Radio%20Telescope/Carleton_T1.pdf [Accessed Aug. 2023].

Clayton, N. (2013). Determination of the Distance to the Galactic Centre. *Diffusion: the UCLan Journal of Undergraduate Research*, [online] 6(1). Available at: https://diffusion.uclan.ac.uk/wp-content/uploads/2019/08/67-180-1-SM.pdf [Accessed Aug. 2023].

Cline, J.D., Castelaz, M. and Clavier, D. (2006). Pisgah Astronomical Research Institute. *Bulletin of the American Astronomical Society*, [online] 38, p.1108. Available at: https://ui.adsabs.harvard.edu/abs/2006AAS...20915401C/abstract [Accessed Jul. 2023].

Cline, J.D., Goldsmith, B., Castelaz, M., Brady, K., DeLisle, T., Owen, L., Steiner, K. and Krochmal, M. (2018). Radio Observations of the 21 August 2017 Solar Eclipse. *American Astronomical Society, AAS Meeting #231*, [online] 242.03. Available at: https://ui.adsabs.harvard.edu/abs/2018AAS...23124203C/abstract [Accessed 2 Sep. 2023].

Condon, J.J. and Ransom, S.M. (2016). *Essential Radio Astronomy*. SCH - School edition ed. [online] Princeton University Press. doi:https://doi.org/10.2307/j.ctv5vdcww.

DK Publishing and Rees, M. (2020). *Universe*. [online] Penguin. Available at: https://books.apple.com/us/book/universe/id1515266186 [Accessed Mar. 2023].

E. Battaner and Florido, E. (2000). The Rotation curve of spiral galaxies and its cosmological implications. *Fundamentals of Cosmic Physics*, [online] 21, pp.1–154. doi:https://doi.org/10.48550/arXiv.astro-ph/0010475.

East Asian Observatory (2014). *Velocity Considerations | Velocity Reference Frame*. [online] James Clerk Maxwell Telescope. Available at: https://www.eaobservatory.org/jcmt/instrumentation/heterodyne/velocity-considerations/.

Eilers, A.-C., Hogg, D.W., Rix, H.-W. and Ness, M.K. (2019). The Circular Velocity Curve of the Milky Way from 5 to 25 kpc. *The Astrophysical Journal*, [online] 871(1), p.120. doi:https://doi.org/10.3847/1538-4357/aaf648.

European Space Agency (2019). *Hubble & Gaia accurately weigh the Milky Way*. [online] ESA Hubble Space Telescope. Available at: https://esahubble.org/news/heic1905/?lang [Accessed Aug. 2023].

Ewen, H.I. and Purcell, E.M. (1951). Observation of a Line in the Galactic Radio Spectrum: Radiation from Galactic Hydrogen at 1,420 Mc./sec. *Nature*, [online] 168(4270), p.356. doi:https://doi.org/10.1038/168356a0.

Fowler, M. (2014). *Maxwell's Equations and Electromagnetic Waves*. [online] Physics Research at the University of Virginia. Available at: http://galileo.phys.virginia.edu/classes/109N/more_stuff/Maxwell_Eq.html [Accessed Aug. 2023] .

Frommert, H. and Kronberg, C. (n.d.). *The Milky Way Galaxy*. [online] The Messier Catalog - Students for the Exploration and Development of Space. Available at: http://www.messier.seds.org/more/mw.html [Accessed 2 Sep. 2023].

Ghigo, F. (2002). *GBT LO Doppler Tracking | Velocity Reference Frames*. [online] *www.gb.nrao.edu*. Green Bank Observatory. Available at: https://www.gb.nrao.edu/~fghigo/gbtdoc/doppler.html [Accessed Aug. 2023].

Gillessen, S., Eisenhauer, F., Trippe, S., Alexander, T., Genzel, R., Martins, F. and Ott, T. (2009). Monitoring Stellar Orbits around the Massive Black Hole in the Galactic Center. *The Astrophysical Journal*, 692(2), pp.1075–1109. doi:https://doi.org/10.1088/0004-637x/692/2/1075.

Giuliani, A. (2005). *Gamma-Ray Emission from the Galactic Plane: a New Model for AGILE*. [Doctoral Thesis] pp.11–17. Available at: http://www.iasf-milano.inaf.it/~giuliani/public/thesis/ [Accessed Aug. 2023].

Gonzalez, O.A. and Gadotti, D.A. (2016). The Milky Way Bulge: Observed Properties and a Comparison to External Galaxies. *Astrophysics and Space Science Library*, 418, pp.199–232, Ch.2. doi:https://doi.org/10.1007/978-3-319-19378-6_9.

Gould, A. (2017). *Johannes Kepler: His Life, His Laws and Times*. [online] NASA. Available at: https://www.nasa.gov/kepler/education/johannes [Accessed Aug. 2023].

Hellwig, H., Vessot, R.F.C., Levine, M.W., Zitzewitz, P.W., Allan, D.W. and Glaze, D.J. (1970). Measurement of the Unperturbed Hydrogen Hyperfine Transition Frequency. *IEEE Transactions on Instrumentation and Measurement*, [online] 19(4), pp.200–209. doi:https://doi.org/10.1109/tim.1970.4313902.

Honma, M., Nagayama, T., Ando, K., Bushimata, T., Choi, Y.K., Handa, T., Hirota, T., Imai, H., Jike, T., Kim, M.K., Kameya, O., Kawaguchi, N., Kobayashi, H., Kurayama, T., Kuji, S., Matsumoto, N.,

Manabe, S., Miyaji, T., Motogi, K. and Nakagawa, A. (2012). Fundamental Parameters of the Milky Way Galaxy Based on VLBI Astrometry. *Publications of the Astronomical Society of Japan*, 64(6), p.136. doi:https://doi.org/10.1093/pasj/64.6.136.

Honma, M. and Yoshiaki Sofue (1997). Rotation Curve of the Galaxy. *Publications of the Astronomical Society of Japan*, [online] 49(4), pp.453–460. doi:https://doi.org/10.1093/pasj/49.4.453.

Hum, S.V. (n.d.). *Noise in Radio Systems*. [online] *ECE422 Lecture Notes*, University of Toronto, pp.1–5. Available at: https://www.waves.utoronto.ca/prof/svhum/ece422/notes/21-noise.pdf.

Imamura, J. (n.d.). *Kirchhoff's Laws | Lecture 4*. [online] Astronomy 122: Birth, Life, and Death of Stars. Available at: https://pages.uoregon.edu/imamura/122/lecture-4/kirchhoff.html [Accessed Aug. 2023].

Imamura, J. (n.d.). *Mass of the Milky Way Galaxy | Lecture 2*. [online] Astronomy 123: Cosmology and Our Place in the Universe. Available at: https://pages.uoregon.edu/imamura/123cs/lecture-2/mass.html [Accessed Aug. 2023].

Institute of Physics (n.d.). *Maxwell's Equations*. [online] Explore Physics. Available at: https://www.iop.org/explore-physics/big-ideas-physics/maxwells-equations#gref.

International Astronomical Union (2012). *RESOLUTION B1 on Guidelines for the Designations and Specifications of Optical and Infrared Astronomical Photometric passbands. Proposed by IAU Commission 25*. [online] Available at: https://www.iau.org/static/resolutions/IAU2012_English.pdf [Accessed Aug. 2023].

International Telecommunications Union (2022). *Radio Noise | Recommendation ITU-R P.372-16 - P Series - Radiowave Propagation*. [online] Radiocommunication Sector of ITU, pp.1–23. Available at: https://www.itu.int/dms_pubrec/itu-r/rec/p/R-REC-P.372-16-202208-I!!PDF-E.pdf [Accessed Aug. 2023].

Jafree, H., Polen, R., Woolard, D. and Dominguez, R. (2022). *The Rotation Curve of the Milky Way Galaxy as Evidence for Dark Matter (PDF)*. [online] *Society of Physics Students*. Available at: https://spsnational.org/file/912606/download?token=v89B-pQz#page=3 [Accessed Aug. 2023].

Jansky, K.G. (1933). Radio Waves from Outside the Solar System. *Nature*, [online] 132(3323), p.66. doi:https://doi.org/10.1038/132066a0.

Jones, B. and Saha, P. (2007). *THE GALAXY Notes for Lecture Courses ASTM002 and MAS430*. [online] *University of Maryland*, Queen Mary University of London, pp.1–15, 61–75, 88–90. Available at: https://www.astro.umd.edu/~richard/ASTRO620/QM_chap1.pdf [Accessed Mar. 2023].

Kalnajs, A.J. (1987). Halos and Disk Stability. *Symposium - International Astronomical Union*, [online] 117(A87-30805 12-90), pp.289–299. doi:https://doi.org/10.1017/s0074180900150375.

Kerr, F.J. and Lynden-Bell, D. (1986). Review of Galactic Constants. *Monthly Notices of the Royal Astronomical Society*, 221(4), pp.1023–1038. doi:https://doi.org/10.1093/mnras/221.4.1023.

King, B. (2019). *Right Ascension & Declination: Celestial Coordinates for Beginners*. [online] Sky & Telescope. Available at: https://skyandtelescope.org/astronomy-resources/right-ascension-declination-celestial-coordinates/ [Accessed Aug. 2023].

Kohler, S. (2016). *Determining Our Motion through the Galaxy*. [online] AAS Nova | Research Highlights from the Journals of the American Astronomical Society. Available at: https://aasnova.org/2016/12/14/determining-our-motion-through-the-galaxy/ [Accessed Aug. 2023].

Kraus, J. (1982). The First 50 Years of Radio Astronomy. *Cosmic Search*, [online] 4(1), pp.p.12-16. Available at: http://www.bigear.org/CSMO/HTML/CS13/cs13p14.htm [Accessed Aug. 2023].

Lemley, C. and Castelaz, M.W. (2014). Design and Construction of a New 1420 MHz Receiver System for a 12-meter Radio Telescope. *American Astronomical Society, AAS Meeting #223*, [online] 148.29. Available at: https://ui.adsabs.harvard.edu/abs/2014AAS...22314829L/abstract [Accessed 2 Sep. 2023].

Library of Congress. (n.d.). *The Milky Way: One of the Many Galaxies | Modeling the Cosmos | Articles and Essays | Finding Our Place in the Cosmos: From Galileo to Sagan and Beyond | Digital Collections* . [online] Available at: https://www.loc.gov/collections/finding-our-place-in-the-cosmos-with-carl-sagan/articles-and-essays/modeling-the-cosmos/the-milky-way-one-of-the-many-galaxies [Accessed Aug. 2023].

Lindblad, P.O. (1999). NGC 1365. *Astronomy and Astrophysics Review*, 9(3-4), pp.221–271. doi:https://doi.org/10.1007/s001590050018.

Liu, L. and Chronopoulos, C. (2008). *The Hydrogen 21-cm Line and Its Applications to Radio Astrophysics*. [online] Massachusetts Institute of Technology. Available at: https://web.mit.edu/lululiu/Public/8.14/21cm/21cm.pdf [Accessed Aug. 2023].

Luzum, B., Capitaine, N., Fienga, A., Folkner, W., Fukushima, T., Hilton, J., Hohenkerk, C., Krasinsky, G., Petit, G., Pitjeva, E., Soffel, M. and Wallace, P. (2011). The IAU 2009 system of astronomical constants: the report of the IAU working group on numerical standards for Fundamental Astronomy. *Celestial Mechanics and Dynamical Astronomy*, [online] 110(4), pp.293–304. doi:https://doi.org/10.1007/s10569-011-9352-4.

M. Lopez-Corredoira, A. Cabrera-Lavers, Mahoney, T.J., Hammersley, P.L., F. Garzón and C. González-Fernández (2006). The Long Bar in the Milky Way: Corroboration of an Old Hypothesis. *The Astronomical Journal*, [online] 133(1), pp.154–161. doi:https://doi.org/10.1086/509605.

Martinez-Medina, L.A., Pichardo, B. and Peimbert, A. (2020). The imprint of arms and bars on rotation curves: in-plane and off-plane. *Monthly Notices of the Royal Astronomical Society*, [online] 496(2), pp.1845–1856. doi:https://doi.org/10.1093/mnras/staa1677.

Mihos, C. (n.d.). *The Solar Motion*. [online] ASTR 222 - Galaxies and Cosmology | Department of Astronomy | Case Western Reserve University. Available at: http://burro.case.edu/Academics/Astr222/Galaxy/Kinematics/solarmotion.html [Accessed Aug. 2023].

Miller, D.F. (1998). *Basics of Radio Astronomy for the Goldstone-Apple Valley Radio Telescope*. [online] *Basics of Radio Astronomy*. NASA Jet Propulsion Laboratory | California Institute of Technology. Available at: https://www2.jpl.nasa.gov/radioastronomy/ [Accessed Aug. 2023].

Mingmuang, Y., Tummuangpak, P., Asanok, K. and Jaroenjittichai, P. (2019). The Mass Distribution and the Rotation Curve of the Milky Way Galaxy Using NARIT 4.5 M Small Radio Telescope and the 2.3 M Onsala Radio Telescope. *Journal of Physics: Conference Series*, 1380(012028). doi:https://doi.org/10.1088/1742-6596/1380/1/012028.

Mróz, P., Udalski, A., Skowron, D.M., Skowron, J., Soszyński, I., Pietrukowicz, P., Szymański, M.K., Poleski, R., Kozłowski, S. and Ulaczyk, K. (2019). Rotation Curve of the Milky Way from Classical Cepheids. *The Astrophysical Journal*, 870(1), p.L10. doi:https://doi.org/10.3847/2041-8213/aaf73f.

NASA (2008). *Orbits and Kepler's Laws | NASA Solar System Exploration*. [online] NASA Solar System Exploration. Available at: https://solarsystem.nasa.gov/resources/310/orbits-and-keplers-laws/ [Accessed Aug. 2023].

NASA (2013). *Discovering the Electromagnetic Spectrum*. [online] Goddard Space Flight Center | Imagine the Universe. Available at: https://imagine.gsfc.nasa.gov/science/toolbox/history_multiwavelength1.html [Accessed Aug. 2023].

NASA (n.d.). *Reference Systems - Basics of Space Flight p.1-3*. [online] NASA Solar System Exploration. Available at: https://solarsystem.nasa.gov/basics/chapter2-1/ [Accessed Aug. 2023].

National Radio Astronomy Observatory (n.d.). *Ewen-Purcell Horn*. [online] Green Bank Observatory. Available at: https://www.gb.nrao.edu/fgdocs/HI21cm/ephorn.html [Accessed Aug. 2023].

National Radio Astronomy Observatory (n.d.). *Prediction of 21 Cm Line Radiation*. [online] Green Bank Observatory. Available at: https://www.gb.nrao.edu/fgdocs/HI21cm/21cm.html [Accessed Aug. 2023].

National Radio Astronomy Observatory (n.d.). *The History of Radio Astronomy*. [online] National Radio Astronomy Observatory. Available at: https://public.nrao.edu/radio-astronomy/the-history-of-radio-astronomy/ [Accessed Aug. 2023].

National Radio Astronomy Observatory (2017). *What Are Radio Telescopes? - National Radio Astronomy Observatory*. [online] National Radio Astronomy Observatory. Available at: https://public.nrao.edu/telescopes/radio-telescopes/ [Accessed Aug. 2023].

National Radio Astronomy Observatory (2022). *The Technology of Radio Astronomy*. [online] Radio Astronomy. Available at: https://public.nrao.edu/radio-astronomy/the-technology-of-radio-astronomy/ [Accessed Aug. 2023].

National Radio Astronomy Observatory. (2020). *Spectral Line — Commonly Used Observing Modes — Guide to Observing with the VLA*. [online] Available at: https://science.nrao.edu/facilities/vla/docs/manuals/obsguide/modes/line [Accessed Aug. 2023].

Nave, C.R. (n.d.). *Gravity Concepts and Applications*. [online] HyperPhysics | Georgia State University. Available at: http://hyperphysics.phy-astr.gsu.edu/hbase/grav.html#grav [Accessed Aug. 2023].

Nave, C.R. (n.d.). *Low Speed Doppler Shift*. [online] HyperPhysics | Georgia State University. Available at: http://hyperphysics.phy-astr.gsu.edu/hbase/Relativ/reldop3.html#c2 [Accessed Aug. 2023].

Nave, C.R. (n.d.). *Relativistic Doppler Effect*. [online] HyperPhysics | Georgia State University. Available at: http://hyperphysics.phy-astr.gsu.edu/hbase/Relativ/reldop2.html#c2 [Accessed Aug. 2023].

Nave, C.R. (n.d.). *The Hydrogen 21-cm Line*. [online] HyperPhysics | Georgia State University. Available at: http://hyperphysics.phy-astr.gsu.edu/hbase/quantum/h21.html [Accessed Aug. 2023].

O'Connor, J.J. and Robertson, E.F. (2006). *Ismael Boulliau - Biography*. [online] MacTutor. Available at: https://mathshistory.st-andrews.ac.uk/Biographies/Boulliau/ [Accessed Aug. 2023].

Olling, R.P. and Merrifield, M.R. (1998). Refining the Oort and Galactic constants. *Monthly Notices of the Royal Astronomical Society*, 297(3), pp.943–952. doi:https://doi.org/10.1046/j.1365-8711.1998.01577.x.

Öpik, E. (1922). An estimate of the distance of the Andromeda Nebula. *The Astrophysical Journal*, [online] 55, pp.406–410. doi:https://doi.org/10.1086/142680.

Palma, C. (n.d.). *The Rotation Curve of the Milky Way | Astronomy 801: Planets, Stars, Galaxies, and the Universe*. [online] www.e-education.psu.edu. Available at: https://www.e-education.psu.edu/astro801/content/l8_p8.html [Accessed Aug. 2023].

Pisgah Astronomical Research Institute (n.d.). *Our History*. [online] Pisgah Astronomical Research Institute. Available at: https://www.pari.edu/about/our-history/ [Accessed 2 Sep. 2023].

Posti, L. and Helmi, A. (2019). Mass and shape of the Milky Way's dark matter halo with globular clusters from Gaia and Hubble. *Astronomy & Astrophysics*, 621(A56). doi:https://doi.org/10.1051/0004-6361/201833355.

Purcell, E.M. (1953). Line Spectra in Radio Astronomy. *Proceedings of the American Academy of Arts and Sciences*, [online] 82(7), p.347. doi:https://doi.org/10.2307/20023736.

Purdue University College of Science (n.d.). *Emission Spectrum of Hydrogen, Explanation of the Emission Spectrum*. [online] Development of Current Atomic Theory. Available at: https://chemed.chem.purdue.edu/genchem/topicreview/bp/ch6/bohr.html#exphyd [Accessed Aug. 2023].

R. Fux (2005). The Galactic Bar. *Kluwer Academic Publishers eBooks*, [online] 315, pp.213–220. doi:https://doi.org/10.1007/1-4020-2620-x_43.

Reid, M.J. (1993). The Distance to the Center of the Galaxy. *Annual Review of Astronomy and Astrophysics*, [online] 31(1), pp.345–372. doi:https://doi.org/10.1146/annurev.aa.31.090193.002021.

Reid, M.J., Menten, K.M., Brunthaler, A., Zheng, X.W., Dame, T.M., Xu, Y., Li, J., Sakai, N., Wu, Y., Immer, K., Zhang, B., Sanna, A., Moscadelli, L., Rygl, K.L.J., Bartkiewicz, A., Hu, B., Quiroga-Nuñez, L.H. and van Langevelde, H.J. (2019). Trigonometric Parallaxes of High-mass Star-forming Regions: Our View of the Milky Way. *The Astrophysical Journal*, 885(2), p.131. doi:https://doi.org/10.3847/1538-4357/ab4a11.

Reid, M.J., Menten, K.M., Zheng, X.W., Brunthaler, A., Moscadelli, L., Xu, Y., Zhang, B., Sato, M., Honma, M., Hirota, T., Hachisuka, K., Choi, Y.K., Moellenbrock, G.A. and Bartkiewicz, A. (2009). Trigonometric Parallaxes of Massive Star-forming Regions. VI. Galactic Structure, Fundamental Parameters, and Noncircular Motions. *The Astrophysical Journal*, 700(1), pp.137–148. doi:https://doi.org/10.1088/0004-637x/700/1/137%20%20%20%20%20 [arXiv:0902.3913].

Reid, M.J., Readhead, A.C.S., Vermeulen, R.C. and Treuhaft, R.N. (1999). The Proper Motion of Sagittarius A*. I. First VLBA Results. *The Astrophysical Journal*, [online] 524(2), pp.816–823. doi:https://doi.org/10.1086/307855.

Rogers, A. and Kimball, L. (1999). *SRT Memo #006*. [online] *Measurement of Galactic rotation curve using 21-cm hydrogen emission Background material*. Massachusetts Institute of Technology Haystack Observatory. Available at: https://www.haystack.mit.edu/wp-content/uploads/2020/07/memo_SRT_006.pdf [Accessed Aug. 2023].

Slipher, V.M. (1914). The Detection of Nebular Rotation. *Lowell Observatory Bulletin No. 62*, [online] 2(12), p.66. Available at: https://articles.adsabs.harvard.edu/full/1914LowOB...2...66S [Accessed Mar. 2023].

Sloan Digital Sky Survey (n.d.). *Energy Levels in Atoms*. [online] SkyServer. Available at: http://cas.sdss.org/DR5/en/proj/advanced/spectraltypes/energylevels.asp [Accessed Aug. 2023].

Sofue, Y. (2011). Accuracy Diagrams for the Galactic Rotation Curve and Kinematical Distances. *Publications of the Astronomical Society of Japan*, [online] 63(4), pp.813–821. doi:https://doi.org/10.1093/pasj/63.4.813.

Sofue, Y. (2013). Rotation Curve and Mass Distribution in the Galactic Center —From Black Hole to Entire Galaxy—. *Publications of the Astronomical Society of Japan*, [online] 65(6), p.118. doi:https://doi.org/10.1093/pasj/65.6.118.

Sofue, Y. (2016). Rotation and Mass in the Milky Way and Spiral Galaxies. *Publications of the Astronomical Society of Japan*, [online] 69(1), p.R1. doi:https://doi.org/10.1093/pasj/psw103.

Sofue, Y. (2020). Rotation Curve of the Milky Way and the Dark Matter Density. *ArXiv (Cornell University)*, (Galaxies: Debate on the Physics of Galactic Rotation and the Existence of Dark Matter). doi:https://doi.org/10.48550/arxiv.2004.11688.

Stephan, K.D. (1999). How Ewen and Purcell Discovered the 21-cm Interstellar Hydrogen Line. *IEEE Antennas and Propagation Magazine* , 41(1), pp.7–17. doi:https://doi.org/10.1109/74.755020 .

Strobel, N. (2022). *Deriving the Galactic Mass from the Rotation Curve*. [online] Strobel's Astronomy Notes. Available at: https://www.astronomynotes.com/ismnotes/s7.htm [Accessed Aug. 2023].

Swinburne University of Technology (n.d.). *Equatorial Coordinate System | COSMOS*. [online] COSMOS - the SAO Encyclopedia of Astronomy. Available at: https://astronomy.swin.edu.au/cosmos/e/equatorial+coordinate+system [Accessed Aug. 2023].

Swinburne University of Technology (n.d.). *Galactic Coordinate System* . [online] COSMOS - the SAO Encyclopedia of Astronomy. Available at: https://astronomy.swin.edu.au/cosmos/G/Galactic+Coordinate+System [Accessed Aug. 2023].

Swinburne University of Technology (n.d.). *Horizontal Coordinate System*. [online] COSMOS - the SAO Encyclopedia of Astronomy . Available at: https://astronomy.swin.edu.au/cosmos/H/Horizontal+Coordinate+System [Accessed Aug. 2023].

Swinburne University of Technology (n.d.). *Parsec*. [online] COSMOS - The SAO Encyclopedia of Astronomy. Available at: https://astronomy.swin.edu.au/cosmos/p/Parsec [Accessed Aug. 2023].

Swinburne University of Technology (n.d.). *Radial velocity*. [online] COSMOS - the SAO Encyclopedia of Astronomy -. Available at: https://astronomy.swin.edu.au/cosmos/r/Radial+velocity [Accessed Aug. 2023].

Swinburne University of Technology (n.d.). *Spin-flip Transition*. [online] COSMOS - The SAO Encyclopedia of Astronomy . Available at: https://astronomy.swin.edu.au/cosmos/s/Spin-flip+Transition [Accessed Aug. 2023].

The VLSR Correction. (2013). [online] *MIT Junior Lab 8.13*. Available at: http://web.mit.edu/8.13/www/srt_software/vlsr.pdf [Accessed Aug. 2023].

Theuns, T. (2007). *Dynamics of Galactic Disks | Stars and Galaxies*. [online] Institute for Computational Cosmology at Durham University. Available at: http://icc.dur.ac.uk/~tt/Lectures/Galaxies/TeX/lec/node39.html [Accessed Aug. 2023].

University of Glasgow (n.d.). *Astronomy 1Y* . [online] Introduction to Cosmology. Available at: https://radio.astro.gla.ac.uk/a1cosmology/pw/Part_I_lecture_cosmology.pdf [Accessed Aug. 2023].

University of Nebraska-Lincoln (n.d.). *Hydrogen Energy Levels*. [online] The Nebraska Astronomy Applet Project - Online Labs for Introductory Level Astronomy. Available at: https://astro.unl.edu/naap/hydrogen/levels.html [Accessed Aug. 2023].

Valenti, E., Zoccali, M., Gonzalez, O.A., Minniti, D., Alonso-García, J., Marchetti, E., Hempel, M., Renzini, A. and Rejkuba, M. (2016). Stellar density profile and mass of the Milky Way bulge from VVV data. *Astronomy & Astrophysics*, [online] 587(L6). doi:https://doi.org/10.1051/0004-6361/201527500 .

Van der Hulst, H.C., Muller, C.A. and Oort, J.H. (1954). The Spiral Structure of the Outer Part of the Galactic System Derived from the Hydrogen Emission at 21cm Wave Length. *Bulletin of the Astronomical Institutes of the Netherlands*, [online] XII(452), pp.117–149. Available at: https://articles.adsabs.harvard.edu/pdf/1954BAN....12..117V [Accessed Aug. 2023].

Weisstein, E.W. (n.d.). *Degree*. [online] Wolfram MathWorld. Available at: https://mathworld.wolfram.com/Degree.html [Accessed Aug. 2023].

Westmeier, T. (2023). *Tools - Useful equations for radio astronomy*. [online] CSIRO Australia Telescope National Facility. Available at: https://www.atnf.csiro.au/people/Tobias.Westmeier/tools_hihelpers.php [Accessed Aug. 2023].

Williams, D.R. (2023). *Earth Fact Sheet*. [online] *Goddard Space Flight Centre | Imagine the Universe*. NASA. Available at: https://nssdc.gsfc.nasa.gov/planetary/factsheet/earthfact.html [Accessed Aug. 2023].

Wood, K. (n.d.). *Widths of Spectral Lines*. [online] *Widths of Spectral Lines | Lecture 8*, University of St. Andrews, pp.1–2, 5. Available at: http://www-star.st-and.ac.uk/~kw25/teaching/nebulae/lecture08_linewidths.pdf.

Zwicky, F. (1937a). An International Review of Spectroscopy and Astronomical Physics. *The Astrophysical Journal*, [online] 86(3), pp.218–246. Available at: https://articles.adsabs.harvard.edu/pdf/1937ApJ....86..217Z [Accessed Aug. 2023].

Zwicky, F. (1937b). On the Masses of Nebulae and of Clusters of Nebulae. *The Astrophysical Journal*, 86, p.217. doi:https://doi.org/10.1086/143864.

10.3 Online Tools

1. NED Coordinate Transformation Calculator: https://ned.ipac.caltech.edu/forms/calculator.html

2. GBO Radial Velocity Calculator: www.gb.nrao.edu/cgi-bin/radvelcalc.py

3. Stellarium Planetarium software https://stellarium.org

4. PARI 12-metre control interface: http://12m.pari.edu/select.jsp

5. Arachnoid LaTeX editor and guide: https://arachnoid.com/latex/

6. CodeCogs LaTeX renderer: https://editor.codecogs.com